THESIS FOR THE DEGREE OF DOCTOR OF PHILOSOPHY

A STUDY OF AN INTEGRATED SAFETY SYSTEM FOR THE PROTECTION OF ADULT PEDESTRIANS FROM CAR COLLISIONS

SUNAN HUANG

VEHICLE SAFETY DIVISION
DEPARTMENT OF APPLIED MECHANICS
CHALMERS UNIVERSITY OF TECHNOLOGY
GÖTEBORG, SWEDEN, 2010

A Study of an Integrated Safety System for the Protection of Adult Pedestrians from Car Collisions

SUNAN HUANG
ISBN 978-91-7385-370-5

Doktorsavhandlingar vid Chalmers tekniska högskola
Ny serie nr 3051
ISSN 0346-718X

Vehicle Safety Division
Department of Applied Mechanics
Chalmers University of Technology
SE-412 96 Göteborg,
Sweden
Telephone +46 (0)31-772 1000

Printed in Sweden by
Chalmers Reproservice
Göteborg, Sweden, 2010

A STUDY OF AN INTEGRATED SAFETY SYSTEM FOR THE PROTECTION OF ADULT PEDESTRIANS FROM CAR COLLISIONS

SUNAN HUANG
VEHICLE SAFETY DIVISION, DEPARTMENT OF APPLIED MECHANICS
CHALMERS UNIVERSITY OF TECHNOLOGY

ABSTRACT

This study aimed to evaluate and improve the performance of a newly developed safety system intended to protect pedestrians during frontal car collisions. This system includes a remote sensor system, a contact sensor, a reversible bumper system (RBS), and a reversible hood (RH).

The remote sensor system was evaluated for its ability to detect pedestrians at risk in a vehicular traffic environment. In this assessment, car-pedestrian accident scenarios were analyzed based on the cases selected from the Swedish TRaffic Accident Data Acquisition (STRADA) database. The two most common scenarios were identified as cars entering and leaving intersections, and colliding with pedestrians crossing the road. The accident data for these two scenarios were then investigated in terms of specific factors, such as the trajectory and velocity of the pedestrians and cars involved. Based on the accident data, a mathematical model was presented, and the remote pedestrian sensor system was evaluated using this model.

The contact sensor was analyzed for the temperature-independent measurement of pedestrian impacts. A baseline bumper finite element (FE) model was initially developed and validated using the European New Car Assessment Program (EuroNCAP) lower legform impact tests performed on the production bumper. Based on the baseline bumper model, an improved bumper model was subsequently developed to meet the acceptance requirements of the European Enhanced Vehicle–safety Committee Working Group 17 (EEVC WG17) lower legform impact tests. A lower limb FE model was then developed and used to evaluate further the protective performance of the baseline and improved bumper models. Finally, the contact sensor was incorporated into the improved bumper model, and a performance study was conducted to evaluate its performance in terms of temperature stability and mass sensitivity of the sensor output.

The performance of the RBS was investigated for the protection of pedestrians' lower limbs during bumper collisions. The detailed FE model of a production car front was developed and validated based on the EuroNCAP lower legform impact tests performed on the production car front. Next, a model RBS was developed to replace the original bumper in the car front model. In order to investigate the performance of the RBS, the lower limb model and the EEVC WG17 lower legform model were used to collide with the RBS model of different design configurations under various impact conditions. Finally, the effects of the design parameters on the protective performance of the RBS were calculated using the statistical method for factorial experiment design.

The RH was evaluated and optimized for the prevention of head injuries among adult pedestrians from hood collisions. The car front FE model was validated based on the EuroNCAP adult headform impact tests conducted on the car hood. The baseline RH was subsequently developed from the original hood of the validated car front model. The FE models of a 50^{th} percentile human head and the EEVC WG17 adult headform were used in parallel to evaluate the protective performance of the baseline RH. In order to minimize the Head Injury Criterion (HIC) values of the headform model, the response surface method was applied to optimize the RH in terms of material stiffness, lifting speed and lifted height. Finally, the headform and human head models were once again used to evaluate the protective performance of the optimized RH.

The results of this study indicated that the remote sensor system can detect almost all visible pedestrians in the two most common scenarios in a timely manner when the detection angle is greater than 60 degrees. The contact sensor can also identify pedestrian impacts with the car bumper. Moreover, enhanced sensor output stability and mass sensitivity can be achieved by using a 25 mm rather than 50 mm sensor tube. The RBS performance can be improved by reducing bumper stiffness; however, such performance is impaired in the bumper-deploying process at speeds of 2.5 m/s or greater. Less than 150 mm, the

deployment distance of the RBS has no influence on the bumper protective performance. Compared with the retracted and lifting baseline RH, the lifted baseline RH can definitely minimize the injury parameters of the headform and human head models. When the optimized RH is lifted, the Head Injury Criterion (HIC) values of the headform and human head models are reduced to much lower than 1,000. Thus, the risk of pedestrian head injuries can be prevented as required by EEVC WG17.

Keywords: Traffic Accidents, Pedestrian Protection, Remote Sensor System, Contact Sensor, Reversible Bumper, Reversible Hood

LIST OF PUBLICATIONS

This thesis summarizes the following papers which are referred to in the text by Roman numbers:

I Huang S.N., Yang J.K. and Eklund F. (2008): Evaluation of Remote Pedestrian Sensor System Based on the Analysis of Car-Pedestrian Accident Scenarios, *Safety Science*, 46 (9), pp. 1345-1355

II Huang S.N., Yang J.K. and Fredriksson R. (2008): Performance Analysis of a Bumper-Pedestrian Contact Sensor System by Using FE Models, *International Journal of Crashworthiness*, Vol. 13, No. 2, pp. 149-157

III Huang S.N. and Yang J.K. (2010): A Reversible Bumper System for Protecting Pedestrian Lower Limbs from Car Collisions, *International Journal of Vehicle Design* (in press)

IV Huang S.N. and Yang J.K. (2010): Optimization of a Reversible Hood for Protecting a Pedestrian's Head during Car Collisions, *Accident Analysis and Prevention* (in press)

The co-author, Dr. Jikuang Yang, provided the original idea of this study. The co-author, Mr. Fredrik Eklund provided the concept and requirements of the remote sensor system in Paper I. The co-author, Mr. Rikard Fredriksson provided the concept of the pedestrian contact sensor and conducted the impact tests for the sensor in Paper II. Otherwise, the opinions, findings and conclusions expressed in the publications and this thesis are my own.

ABBREVIATIONS AND NOTATIONS

ACL	Anterior Cruciate Ligament
AIS	Abbreviated Injury Scale
APE	Average Prediction Error
EEVC WG17	European Enhanced Vehicle-safety Committee Working Group 17
ERSO	European Road Safety Observatory
EuroNCAP	European New Car Assessment Program
FE	Finite Element
FMVSS	Federal Motor Vehicle Safety Standards
GDV	German Insurance Association–Institute of Vehicle Safety
GIDAS	German In-Depth Accident Study
HIC	Head Injury Criterion
HUMOS	HUman Model for Safety
IHRA	International Harmonized Research Activities
ITARDA	Institute for Traffic Accident Research and Data Analysis, Japan
LCL	Lateral Collateral Ligament
LLMS	Lower Limb Model for Safety
LOF	Lack Of Fit
MBS	Multi Body System
MCL	Medial Collateral Ligament
NHTSA	National Highway Traffic Safety Administration, USA
PCL	Posterior Cruciate Ligament
RBS	Reversible Bumper System
RH	Reversible Hood
SALi	Shock Absorbing Liquid
SRA	Swedish Road Administration
SSR	Sum of Squared Residuals
STRADA	Swedish TRaffic Accident Data Acquisition
TABC	Traffic Administration Bureau of China
THUMS	Total HUman Model for Safety
ULP	Universite Louis Pasteur
UNECE	United Nations Economic Commission for Europe
WSTC	Wayne State Tolerance Curve
WSUBIM	Wayne State University Brain Injury Model

ACKNOWLEDGEMENTS

This study was carried out at Vehicle Safety Division, Department of Applied Mechanics, Chalmers University of Technology, Göteborg, Sweden and was sponsored by the Intelligent Vehicle Safety Systems (IVSS) Program, Sweden, and European 6th Framework Programme Integrated Project (IP) on Advanced PROtection SYStems (APROSYS).

I would like to thank all those who have helped me throughout this study:

Dr. Jikuang Yang, Associate Professor, Department of Applied Mechanics, Chalmers University of Technology, Sweden, my supervisor, for initializing this study, constant guidance and supervision, insightful suggestion and encouragement throughout this study.

Dr. Yngve Håland, Adjunct Professor, Department of Applied Mechanics, Chalmers University of Technology, Sweden, my co-supervisor, for helpful discussion and valuable suggestion.

Mr. Fredrik Eklund, Product Manager, Autoliv Electronics, Sweden, for his fruitful discussion and effective cooperation.

Mr. Rikard Fredriksson, Research Engineer, Autoliv Research, Sweden, for his informative suggestion and valuable instruction.

Mr. Mark Neal, Research Engineer, GM R&D, U.S., for his valuable discussion and fruitful suggestion.

All my colleagues in GM R&D and GM Saab for their generous help. Especially appreciate Jenne-Tai Wang and Ingemar Söderlund.

Ms. Helen Fagerlind, Project Manager, Department of Applied Mechanics, Chalmers University of Technology, Sweden, for providing valuable accident data.

All my colleagues at the Vehicle Safety Division for a pleasant working atmosphere.

Finally I am very grateful to my family, wife Xin Liu, my son Ruiheng, my parents and my parents-in-law for their immense love and encouragement during my study.

TABLE OF CONTENTS

1. INTRODUCTION

1.1 Background

Although pedestrian safety has improved in highly motorized countries (ERSO, 2008; NHTSA, 2008a), pedestrian casualties remain prominent in traffic accidents. In 2007, 70,000 pedestrians were injured and 4,645 were killed in traffic accidents in the United States, which accounted for 3% of the total traffic injuries and 11% of all traffic fatalities (NHTSA, 2008b). In 2004, 1,582 pedestrians were injured and 67 killed in road traffic accidents in Sweden, which represented 6% of the total traffic injuries and 14% of all traffic fatalities (UNECE, 2007). In 2003, 85,592 pedestrians were injured and 2,332 were killed in traffic accidents in Japan, which accounted for 7% of the total traffic injuries and 30% of all traffic fatalities (ITARDA, 2004). In 2006, 82,391 pedestrians were injured and 23,285 killed in traffic accidents in China, which represented 19% of the total traffic injuries and 26% of all traffic fatalities (TABC, 2007).

Passenger cars are overrepresented in pedestrian traffic accidents. Yang et al. (2005) investigated the types of vehicles involved in pedestrian accidents based on data from the Swedish TRaffic Accident Data Acquisition (STRADA) database. These researchers found that 79.2% of the vehicles involved in accidents were passenger cars. Guo et al. (2006) analyzed the vehicle types in 158 fatal/serious vehicle-pedestrian crashes in Beijing, China, and determined that 51.3% of the vehicles were passenger cars. In 2007, passenger cars accounted for 64% of the vehicles involved in single vehicle-pedestrian crashes in the United States. Furthermore, the car front is the major contact source in pedestrian crashes. In 2007, the initial point of impact in 71% of the passenger car-pedestrian crashes in the United States occurred at the car front (NHTSA, 2008c).

Previous studies have presented several systems intended to protect pedestrians during collisions with the car front. In order to minimize the pedestrians' injuries caused by collisions with the car bumper, a new bumper system was presented that absorbs the impact energy more efficiently (Shuler and Staines, 1998; Kalliske and Friesen, 2001; Chon et al., 2007; Doerr et al., 2007; Jaarda and Nagwanshi, 2007; Pinecki and Zeitouni, 2007; Glance and Tokarz, 2008; Davies et al., 2009). In order to protect pedestrians' heads during impacts with the car hood, the active hood system was implemented to soften such collisions (Fredriksson et al., 2001; Kalliske and Friesen, 2001; Krenn et al., 2003; Lee et al., 2007; Pinecki and Zeitouni, 2007; Oh et al., 2008; Shin et al., 2008; Inomata et al., 2009). In addition to the bumper and hood systems, external airbags were also presented to protect pedestrians from car collisions. Maki and Asai (2002) presented an A-pillar airbag designed to cushion the impact between the pedestrian's head and the A-pillar. Holding et al. (2001) and Moxey et al. (2006) presented a concept which combined the bumper and scuttle airbags to cushion car-pedestrian impacts. Bovenkerk et al. (2009) presented a U-shaped scuttle airbag combined with a pop-up hood intended to protect the pedestrian's head during collisions with the scuttle area, and the lower parts of the windscreen and A-pillar.

Various sensor systems have been presented that serve to detect pedestrian impacts and to trigger pedestrian protective systems. These sensor systems can be divided into two major groups: remote sensor systems and contact sensor systems. Remote sensor systems can detect imminent pedestrian impacts. Typical remote sensor systems include the radar sensor, laser scanner, infrared camera, stereo vision camera and combinations of these devices (Gavrila et al., 2001; Holding et al., 2001; Labayrade et al., 2005; Linzmeier et al., 2005; McCarthy and Simmons, 2005; Moxey et al., 2006; Krotosky and Trivedi, 2007; Chen and Han, 2008; Natroshvili et al., 2008; Gidel et al., 2009). Meanwhile, contact sensor systems can detect and identify pedestrian impacts. Typical contact sensor systems include the accelerometer, piezoelectric sensor, fiber optical sensor and pressure sensor (Zanella et al., 2002; Mlekusch et al., 2004; Kim and Chang, 2005; Scherf, 2005; Lee et al., 2007).

In order to protect pedestrians from collisions with the car front, an integrated safety system was developed as the combination of a reversible bumper system (RBS), a reversible hood (RH), a remote sensor system, and a contact sensor. The RBS is designed as a movable bumper. When the risk of a pedestrian collision is detected, the RBS can be deployed prior to the crash in order to absorb impact energy more efficiently and better protect the pedestrian's lower limbs. If the crash is avoided, the RBS can move back into place to protect against future accidents. The RH functions in a way similar to the RBS. When the risk of a pedestrian collision is detected, the rear end of the RH can be lifted to protect the

pedestrian's head. If the collision is avoided, the lifted rear end can be retracted to protect against future accidents. In order to trigger the RBS and RH, a remote sensor system, which combines a stereo vision sensor and a radar sensor, is included in the integrated safety system to detect upcoming pedestrian impacts. In addition, a pedestrian contact sensor installed in the RBS can also be implemented to reduce instances of false RH deployment. The current study evaluated and improved the performance of the integrated safety system.

1.2 Epidemiology of Pedestrian Accidents

1.2.1 Pedestrian Casualties

Figure 1-1 shows the number of pedestrian casualties, the ratio of pedestrian casualties to total traffic casualties, and the pedestrian mortality in the United States in 2007 (NHTSA, 2008b), specific European countries in 2004 (UNECE, 2007), Japan in 2003 (ITARDA, 2007), and China in 2006 (TABC, 2007). This figure demonstrates that pedestrian casualties account for a significant portion of total traffic casualties, especially in China, Greece, France, and the United Kingdom. The mortality of pedestrian casualties reaches a peak value of 22% in China, which is much higher than the 10% in Greece and the 6% in the United States. Except for France, the mortality of pedestrian casualties is higher than the average mortality of traffic victims, especially in the United States and Japan.

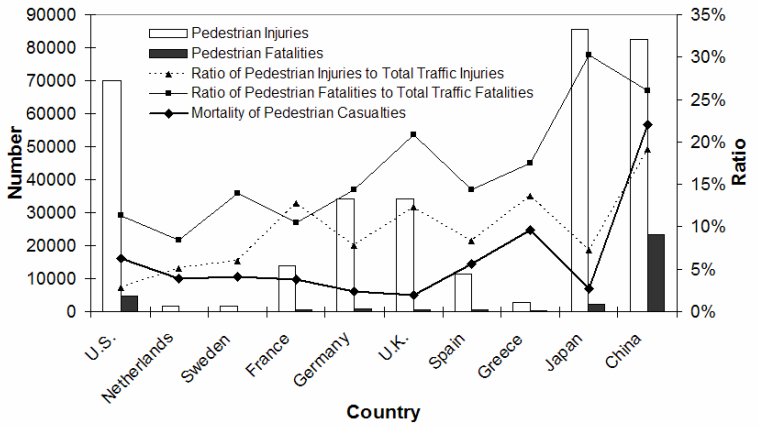

Figure 1-1 Pedestrian casualties (ITARDA, 2004; TABC, 2007; UNECE, 2007; NHTSA, 2008b)

1.2.2 Pedestrian Age and Gender

Figure 1-2 indicates the number of U.S. pedestrians injured and killed in 2007 per 100,000 residents according to age and gender groups. Elderly pedestrians (65 and older) have the highest number of fatalities; however, among injured pedestrians, young people—especially those 10 to 24 years old—are clearly overrepresented. The large number of fatalities among elderly pedestrians can be explained by their reduced mobility, impaired perception to risk, and reduced injury tolerance (Holubowycz, 1995; Oxley, 1997; Harruff et al., 1998; Gorrie et al., 2008; Lobjois and Cavallo, 2009; Holland and Hill, 2010). In comparison, the overrepresentation of injured young pedestrians can result from their insufficient cognition of the traffic environment (Assailly, 1997; Barton and Schwebel, 2007; Zhou and Horrey, 2010) or their greater exposure to traffic (Holland and Hill, 2010). Figure 1-2 also illustrates that fatalities among male pedestrians are much higher than among females. In particular, among pedestrians aged 16 years and older, the number of male pedestrians killed is more than twice that of females. Among injured pedestrians, the disparity caused by gender is not tremendous; however, males are clearly more likely to be injured in traffic accidents, except in a few age groups.

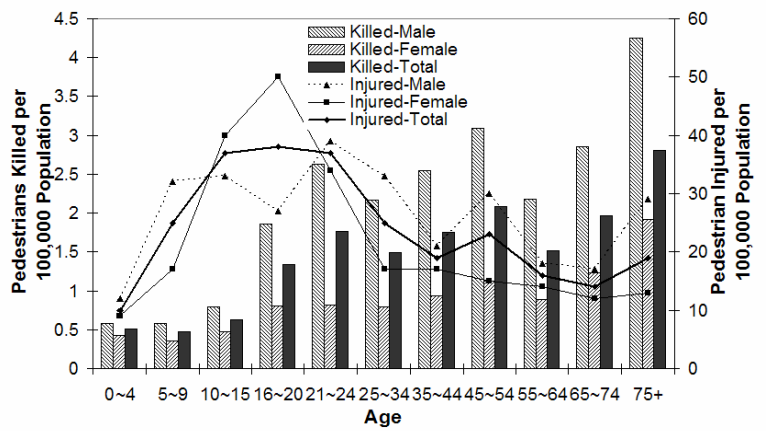

Figure 1-2 Age and gender distribution of pedestrian casualties (NHTSA, 2008c)

1.2.3 Vehicle Involvement

Figure 1-3 indicates the types of vehicles involved in pedestrian accidents. Al-Ghamdi (2002) investigated 638 pedestrian-vehicle crashes in Riyadh, Saudi Arabia from 1997 to 1999, and determined that 66.9% of the vehicles involved in the cases were passenger cars. Trucks represented the second largest portion at 23.8%. Yang et al. (2005) investigated the types of vehicles involved in pedestrian accidents in Sweden from 1999 to 2004, and found that passenger cars accounted for 79.2% of the vehicles involved in the cases studied. The next most prominent vehicle type was bus, which represented 5.6% of the vehicles involved. Meanwhile, Yang and Otte (2007) analyzed the vehicle types involved in 3,603 pedestrian accidents in Changsha, China, from 2001 to 2005. In the Chinese cases, passenger cars accounted for 52% of the vehicles involved, followed by motorcycles at 22% representation. According to NHTSA (2008c) figures in 2007, passenger cars accounted for 64% of the vehicles involved in single vehicle-pedestrian crashes in the United States. The car front was found to be the major contact source in those crashes. In 71% of the passenger car-pedestrian crashes, the initial impact point was on the car front.

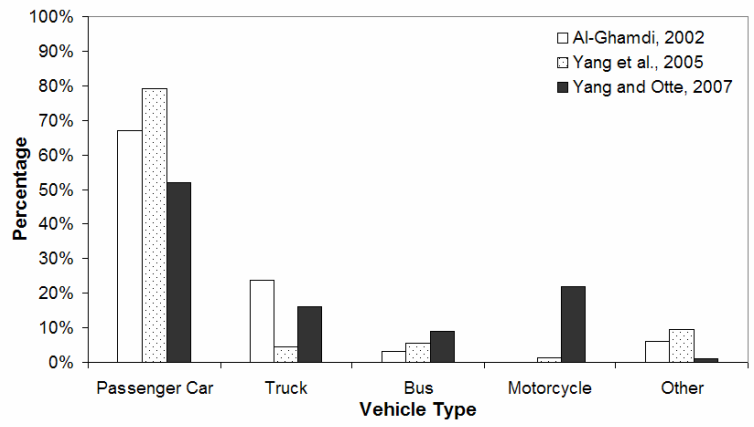

Figure 1-3 Vehicle types in pedestrian accidents (Al-Ghamdi, 2002; Yang et al., 2005; Yang and Otte, 2007)

1.2.4 Pedestrian Injury and Causation

As shown in Figure 1-4a, Mizuno (2005) summarized the actions of the working group of International Harmonized Research Activities (IHRA) relative to pedestrian safety issues by examining pedestrian injuries of Abbreviated Injury Scale (AIS) 2-6 according to body regions and car front contact sources. In addition, Chen et al. (2009) analyzed 200 pedestrian accidents in China in order to compare the results with the IHRA data, as shown in Figure 1-4b. As indicated in Figure 1-4, the head and lower limbs are the most frequently injured parts of the body. According to the IHRA data, 30% of all injuries occurred to the head and 35% to the lower limbs. Based on the data from China, 30% of the injuries occurred to the head and 27% to the lower limbs. Regarding head injuries, the leading contact source is the windscreen glass, which was responsible for 44% of all IHRA head injuries and 76% of the Chinese head injuries. The second source is the bonnet/wing top surface, which caused 29% of all IHRA head injuries and 14% of the

Chinese injuries. In regard to lower limb injuries, the front bumper is the major contact source, which caused 73% of the IHRA lower limb injuries and 75% of the Chinese injuries.

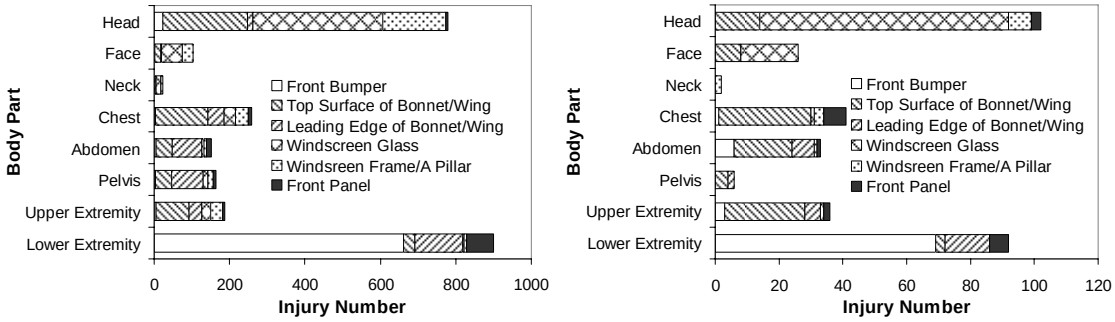

(a) Mizuno, 2005 **(b) Chen et al., 2009**

Figure 1-4 Pedestrian injuries by body parts and car front contact sources

When considering the severe and fatal injuries sustained by pedestrians in car collisions, the head is the most frequently injured body part. Kramlich et al. (2002) investigated the typical characteristics of 1,200 car-pedestrian accidents recorded by the German Insurance Association–Institute of Vehicle Safety (GDV). Considering the pedestrians who were injured to AIS 4+ level, the largest portion (10.3%) of the 688 pedestrians older than 10 years of age suffered AIS 4+ head injuries. This was almost twice the following percentage (5.2%) of the pedestrians injured AIS 4+ on the thorax. Of the 148 pedestrians up to 10 years of age, 8.2% suffered AIS 4+ head injuries—more than four times the following percentage of the pedestrians injured AIS 4+ on the neck (2.0%). Maki et al. (2003) investigated the primary injures that caused fatalities among pedestrians age 13 or older in 4,416 car collisions, and found that 64% of the fatalities resulted from head injuries while 9% were from chest injuries. Yang and Otte (2007) compared passenger-vehicle traffic accidents and injuries among vulnerable road users in China and Germany from 2000 to 2005. They identified that among the 11 Chinese pedestrians who received AIS 4+ injuries, the head was the only part of the body injured, with 9 receiving such AIS 4+ injuries. In the 24 German cases, the head and chest were overrepresented, with 40.5% and 35.1% of all 37 AIS 4+ injuries inflicted on these two body parts, respectively. The windscreen, A-pillar, and hood were identified as the major contact sources associated with severe and fatal head injuries (Foret-Bruno et al., 1998; Mizuno and Kajzer, 2000; Kramlich et al., 2002; Longhitano et al., 2005; Richards et al., 2009).

1.2.5 Impact Speed

The relationship between the risk of pedestrian fatality and the speed of the vehicle upon impact has long been investigated (Ashton, 1980; Anderson et al., 1997; Davis, 2001; Gårder, 2004; Cuerden et al., 2007; Rosen and Sander, 2009; Kong and Yang, 2010). Table 1-1 summarizes some of the statistics on pedestrian fatality risk versus vehicle impact speed. According to Ashton's (1980) results, at speeds ranging from 30 km/h to 50 km/h, the risk of pedestrian fatality increases quickly; and when the vehicle impact speed is greater than 70 km/s, the impacted pedestrian has less chance of survival. Notably, the risk of pedestrian fatality observed by Davis (2001) and Rosen and Sander (2009) at the same vehicle impact speed is much lower than the result seen by Ashton (1980). It was suggested that high speed crashes should be considered in future pedestrian safety design (Rosen and Sander, 2009). Kong and Yang (2010) conducted a study based on real-world accident cases in China. According to their results, the risk of pedestrian fatality at speeds ranging from 30 km/h to 50 km/h is half the result seen by Ashton (1980); at 70 km/h, however, their result is closer to Ashton's (1980) finding.

Table 1-1 Pedestrian fatality risk versus vehicle impact speed

Source	Years of Data	30 km/h	50 km/h	70 km/h
Ashton, 1980	1965~1979	5.0%	45.0%	95.0%
Anderson et al., 1997	1983~1999	8.0%	85.0%	100.0%
Davis, 2001[a]	1965~1979	1.0%	7.0%	51.0%
Rosen and Sander, 2009[b]	2003~2007	1.7%	8.1%	37.0%
Kong and Yang, 2010	2003~2009	2.6%	26.0%	82.0%

[a]The fatality risk was estimated for the pedestrians aged from 15 to 59 years old.
[b]The impact vehicles were only passenger cars.

1.3 Biomechanics of Pedestrian Injuries

According to the epidemiology study of pedestrian accidents, the head and lower limbs are the most frequently injured body parts (Mizuno, 2005; Chen et al., 2009). Therefore, this discussion focuses on the injuries that involve these body parts.

1.3.1 Biomechanics of Head Injuries

The windscreen, A-pillar, and hood have been identified as the major contact sources of severe and fatal head injuries (Foret-Bruno et al., 1998; Mizuno and Kajzer, 2000; Kramlich et al., 2002; Longhitano et al., 2005; Richards et al., 2009). The substantial stiffness of vehicle parts, such as the hood rear and scuttle, the hood-fender edge, the windscreen frame, as well as the rigid accessories in the engine compartment, serves as the main reason for severe head injuries (Mizuno et al., 2001; Yang, 2003; Yang, 2005; Li and Yang, 2007).

The most significant head injuries are skull damage and brain injuries (Wismans et al., 2000; Schmitt et al., 2004; Yang, 2005). Table 1-2 summarizes these injuries and their mechanisms. Skull fractures are caused mainly by excessive local deformation resulting from contact force. Brain injuries are always induced by inertial loads: translational acceleration produces focal brain injuries whereas rotational acceleration causes diffuse brain injuries. When the pedestrian's head is struck by a car front, these three injury mechanisms can occur.

Table 1-2 Common head injuries and mechanisms (Yang, 2005)

Head Injury			Mechanism
Skull	Fracture		Contact force
Brain	Focal	Coup contusion	Contact force
		Contre-coup contusion	Pressure wave
		Epidural hematoma	Contact force
		Subdural hematoma	Translational and rotational acceleration
	Diffuse	Concussion	Translational and rotational acceleration
		Diffuse axonal injury	Rotational motion

Table 1-3 summarizes the results of several studies on the fracture thresholds of the skull to the contact force and the injury tolerances of the brain to the angular acceleration and velocity.

Table 1-3 Skull and brain tolerances to impact loads

Body Part		Force (kN)	Angular Acceleration (rad/s^2)	Angular Velocity (rad/s)	Source
Skull	Frontal	3.6-9.0	-	-	Hodgson and Thomas (1971)
	Zygoma	0.5-2.9	-	-	Nahum et al. (1968)
	Temporo-parietal	5.0-12.5	-	-	Allsop et al. (1991)
	Occipital	6.4	-	-	SAE (1980)
	Maxilla	2.0-4.2	-	-	Nyquist et al. (1986)
	Mandible	0.8-3.4	-	-	Schneider and Nahum (1972)
Brain	Cerebrum	-	1800 (t<20 ms)	30 (t>20 ms)	Ommaya et al. (1967)
	Bridging vein	-	4500	70	Löwenhielm (1974)
	Brain surface	-	2000-3000	-	Advani et al. (1982)

The first extensive quantification of head tolerance to translational impact acceleration is evident in the Wayne State Tolerance Curve (WSTC) (see Figure 1-5). This curve was established based on a large number of cadaver tests that focused on head acceleration in order to indicate a relationship between the level of head front-end translational acceleration and the pulse duration for a special level of head injury severity (Gurdjian et al., 1953; Lissner et al., 1960; Gurdjian et al., 1966). A combination of magnitude and duration which lies above the curve is likely to cause AIS 3+ head injuries.

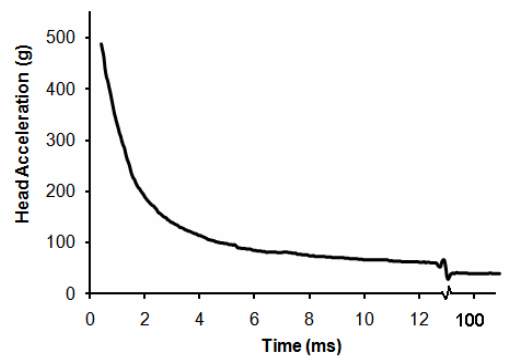

Figure 1-5 WSTC head injury tolerance curve

Versace (1971) proposed a version of the Head Injury Criterion (HIC) as a measure of average acceleration correlated with the WSTC. Responding to the Versace's (1971) study, the National Highway Traffic Safety Administration (NHTSA) defined HIC in 1972 and included it in Federal Motor Vehicle Safety Standards (FMVSS) No. 208. The HIC value is calculated using the following equation:

$$HIC = \max\left[\frac{1}{t_2 - t_1}\int_{t_1}^{t_2} a(t)dt\right]^{2.5}(t_2 - t_1) \qquad 1\text{-}1$$

where t_1 and t_2 are two arbitrary times (in seconds) from the duration of the acceleration pulse and $a(t)$ is the resultant head translational acceleration (in g's) measured at the center of head gravity. FMVSS No. 208 requires a maximum time interval of 36 ms; for a 50th percentile male, the HIC36 value should not exceed 1,000. In 2000, NHTSA introduced a 15-ms maximum time interval to calculate the HIC15 value; for the 50th percentile male, the HIC15 value should not be greater than 700 (Eppinger et al., 2000).

1.3.2 Biomechanics of Lower Limb Injuries

The bumper is the leading source of lower limb injuries (Mizuno, 2005; Chen et al., 2009). Pedestrians' typical lower limb injuries include fractures of long bones (femur, tibia, and fibula), damage to the knee joint (such as the ligament avulsion and the condyle fracture), and ankle/foot dislocation and fracture (Foret-Bruno et al., 1998; Edwards and Green, 1999; Yang, 2005).

The primary mechanism for long bone fractures has been identified as the shearing and bending loads induced by bumper and/or hood leading-edge impacts (Nahum and Melvin, 2001). The fracture tolerances of the femur, tibia, and fibula are summarized from previous studies in Table 1-4. Furthermore, the failure forces of long bones depend on impact speed: the greater the impact speed, the larger the impact force needed to fracture long bones (Kress et al., 1995; Yang, 1997).

Table 1-4 Breaking tolerances of the femur, tibia, and fibula

Bone	Shearing Force (kN)	Bending Moment (Nm)	Tensile Stress (MPa)	Source
Femur	3.1 (LM)~5.7 (AP)	-	147~284	Kress et al. (1993)
	1.45±0.65 (F, PA)~5.7±2.68 (M, AP)	-	-	Kress et al. (1995)
	1.31~8.37	100~500	-	Kress and Porta (2001)
	-	120~440	-	Ivarsson et al. (2009)
Tibia	3.3~4.3	-	-	Krammer et al. (1973)
	1.0	-	-	Bunketorp et al. (1982)
	4.1±1.2 (F), 4.7±1.4 (M)	278±30 (F), 317±88 (M)	94~435	Nyquist et al. (1985)
	-	241±49 (S), 408±115 (D)	-	Schreiber et al. (1997)
	1.02±0.35 (M, LM)~4.85±2.08 (M, AP)	-	-	Kress et al. (1995)
	1.19~7.07	100~500	-	Kress and Porta (2001)
Fibula	0.57±0.28 (F, LM)~2.15±1.27 (M, AP)	-	-	Kress et al (1995)

F: female; M: male. LM: lateral-to-medial; AP: anterior-to-posterior. S: static; D: dynamic.

Knee injuries are caused mainly by the contact force resulting from the direct impact on the knee and the forces transferred through the knee joint. Knee injuries caused by direct contact force include fractures of the fibula head and lateral tibia condyle, extra-articular injuries, and diaphyseal fractures of the tibia or femur. These injuries always occur at the beginning stage of lateral knee displacement (Kajzer et al.,

1990). The forces transferred through the knee joint can result in the shearing and bending deformation of the knee joint. Knee-shearing dislocation generates the tension in knee ligaments and the concentrated contact force between the medial femur condyle and the tibial intercondylar eminence. If the tolerance level is exceeded, then the ligaments can be avulsed, the tibial intercondylar eminence can be fractured, and the femoral cartilage can also be damaged (Kajzer et al., 1990). When the knee joint is exposed to a bending load, the knee ligaments are stretched, and the compressing force is induced between lateral condyles. The excessive bending of the knee joint leads chiefly to partial or total rupture of Medial Collateral Ligament (MCL). However, the fracture of the tibia condyle and the rupture of Lateral Collateral Ligament (LCL), Anterior Collateral Ligament (ACL), and Posterior Collateral Ligament (PCL) can also occur (Kajzer et al., 1993). The injury tolerances of the knee joint have been investigated in several studies and are summarized in Table 1-5.

Table 1-5 Injury tolerances of the knee joint

Shearing Force (kN)	Bending Moment (Nm)	Test Condition	Source
0.75~3	100	Quasi-static	Remet et al. (1995)
1.8±0.4	-	15 km/h	Kajzer et al. (1990)
2.6±0.5	-	20 km/h	
-	101±21	16 km/h	Kajzer et al. (1993)
-	123±35	20 km/h	
2.4±0.2	418±100	20 km/h, pure shearing	Kajzer et al. (1999)
1.3±0.5	307±147	20 km/h, pure bending	
2.6±0.5	489±141	40 km/h, pure shearing	Kajzer et al. (1997)
1.5±0.6	331±79	40 km/h, pure bending	

1.4 Countermeasures for Pedestrian Protection

Several systems have been developed to protect pedestrians from crashes with the car front. In order to alleviate the injuries to pedestrians caused by collisions with the car bumper, a new bumper system was developed that absorbs impact energy more efficiently. The basic design of the energy absorption bumper includes an energy absorber made of plastics, foam, or Shock Absorbing Liquid (SALi). This absorber is located between the bumper beam and the bumper cover to absorb impact energy (Shuler and Staines, 1998; Kalliske and Friesen, 2001; Chon et al., 2007; Doerr et al., 2007; Jaarda and Nagwanshi, 2007; Pinecki and Zeitouni, 2007; Glance and Tokarz, 2008; Davies et al., 2009). Strengthening and moving the lower stiffener forward have also been considered as a feasible method to dissipate part of the impact energy and reduce knee bending (Shuler and Staines, 1998; Chon et al., 2007; Doerr et al., 2007; Pinecki and Zeitouni, 2007).

In order to protect the pedestrian's head from collisions with the car hood, the active hood system (see Figure 1-6) was implemented to soften such collisions (Fredriksson et al., 2001; Kalliske and Friesen, 2001; Krenn et al., 2003; Lee et al., 2007; Pinecki and Zeitouni, 2007; Oh et al., 2008; Shin et al., 2008; Inomata et al., 2009). This system consists of a hood that lifts at the rear when a pedestrian is struck by the car. In this case, the distance between the hood and the stiff inner parts of the car (e.g., the engine) becomes wider, creating a larger degree of hood deformation when the hood is struck by the pedestrian's head. As a result, more impact energy can be absorbed and head injuries can be alleviated.

Figure 1-6 Active hood in the lifted position (Fredriksson et al., 2001)

In addition to the energy absorption bumper and active hood, external airbags are also used to soften car-pedestrian impacts. Maki and Asai (2002) presented an A-pillar airbag to cushion the pedestrian's head impacted with the A-pillar. Holding et al. (2001) and Moxey et al. (2006) presented a concept to combine bumper and scuttle airbags in order to cushion the pedestrian's body impacted by the car front. Bovenkerk et al. (2009) presented a U-shaped scuttle airbag combined with a pop-up hood to protect the pedestrian's head from collisions with the scuttle area, as well as the lower parts of the windscreen and A-pillar. Figure 1-7 illustrates a car equipped with the U-shaped scuttle airbag and pop-up hood. If an unavoidable pedestrian impact is detected, the U-shaped airbag is triggered to cover the scuttle area, as well as the lower parts of the windscreen and A-pillar. Simultaneously, the pop-up hood will be lifted by the deploying airbag. Through this combination of airbag and pop-up hood, the pedestrian's head can be protected during collisions that are often severe and even fatal.

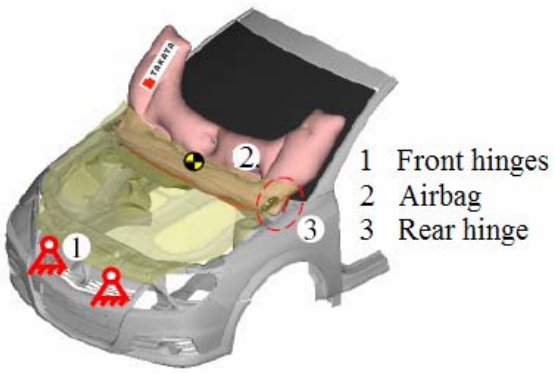

Figure 1-7 U-shaped scuttle airbag and pop-up hood (Bovenkerk et al., 2009)

1.5 Sensor Systems to Detect Pedestrian Crashes

In order to trigger the protective systems, various sensor systems are used to detect pedestrian impacts. These systems can be divided into two major groups: remote sensor systems and contact sensor systems.

1.5.1 Remote Sensor Systems

Remote sensor systems can detect upcoming pedestrian impacts. Typical remote sensors used to detect pedestrian crashes include the radar sensor, laser scanner, infrared camera, and stereo vision camera (Gavrila et al., 2001; Holding et al., 2001; Labayrade et al., 2005; Linzmeier et al., 2005; McCarthy and Simmons, 2005; Moxey et al., 2006; Krotosky and Trivedi, 2007; Chen and Han, 2008; Natroshvili et al., 2008; Gidel et al., 2009). The characteristics of these sensors are compared in Table 1-6.

Table 1-6 Comparison of remote sensors for pedestrian detection (Gandhi and Trivedi, 2006)

Sensor Type	Detection Method	Detected Information	View Field	Angular Resolution	Detection Range	Range Resolution
Radar	Radar wave	Speed and distance	Narrow	Low	Low/medial	High
Laser Scanner	Laser pulse	Speed and distance	Wide	Medial	Medial	High
Infrared Camera	Infrared radiation	Visual features	Medial	Low/medial	Low/medial	Low
Vision Camera	Visual light	Visual features	Medial	Medial/high	Low/medial	Medial

Compared to radar and laser sensors, infrared and vision cameras provide much richer information about pedestrians and the background environment. However, the image sequences cannot be used without further interpretation (Bu et al., 2005). Based on the image sequences, different methods have been used to identify pedestrians. The two primary trends (Bu et al., 2005) are the shape-based method (Gavrila and Giebel, 2002; Bertozzi et al., 2003; Ramanan et al., 2007) and the motion-based method (Mori et al., 1994; Niyogi and Adelson, 1994; Cutler and Davis, 1999; Fardi et al., 2005). Although radar and laser signals cannot be used to identify pedestrians directly, they can provide accurate location and motion information regarding pedestrian movement. Considering the different characteristics of these sensor systems, the radar sensor and laser scanner are used concurrently with an infrared camera or vision camera to provide more accurate identification and location of pedestrians (Gavrila et al., 2001; Labayrade et al., 2005; Linzmeier et al., 2005; McCarthy and Simmons, 2005; Moxey et al., 2006; Gidel et al., 2009).

1.5.2 Contact Sensor Systems

Contact sensor systems can detect and identify pedestrian impacts as crashes occur. Typical contact sensors include the accelerometer, piezoelectric sensor, fiber optical sensor and pressure sensor (Zanella et al., 2002; Mlekusch et al., 2004; Kim and Chang, 2005; Scherf, 2005; Lee et al., 2007).

A piezoelectric sensor is a device that uses the piezoelectric effect to measure pressure, acceleration, strain, or force. In the application for pedestrian detection, one or more piezoelectric sensors can be integrated into the front of the vehicle, as shown in Figure 1-8, to detect the initial impact. During the collision, the stress detected by the sensor is transformed proportionally into piezoelectricity and processed by the sensor circuit. By analyzing the sensor signal, the effective mass and dimension of the object is identified. According to the preset threshold, the triggering decision is made. Because of the fast dynamic response of the piezoelectric sensor and its far front installation position, the piezoelectric sensor can detect and analyze an impact as soon as it occurs (Zanella et al., 2002; Kim and Chang, 2005).

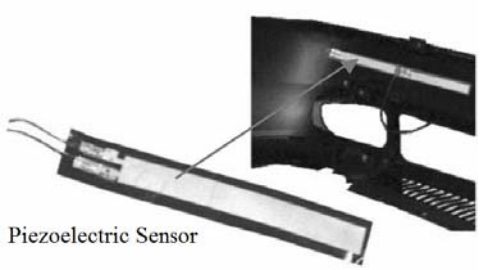

Figure 1-8 Piezoelectric sensor (Zanella et al., 2002)

Scherf (2005) presented a fiber-optic contact sensor for pedestrian impact detection. The entire contact sensor is comprised of 16 fiber-optic segments that detect the flexion caused by the impact. A normal optical fiber is covered by a reflective coating to minimize the loss of light transferring through it. In the contact sensor, that coating is partially removed, thereby inducing a constant loss of light transferring through the straight fibers. This loss can be increased or reduced through the flexion of the fibers. Such a change can be transformed into an electrical signal. Based on this phenomenon, any impact with the bumper can be detected by the attached sensor.

Mlekusch et al. (2004) presented a pressure sensor concept to detect pedestrian impacts. In it, a small tube is fixed on the inner surface of the bumper cover. Both ends of the tube are sealed by a pressure sensor, with air serving as the medium inside the tube. When the bumper is impacted, the sensor tube is compressed and the impact signal is detected by the pressure sensors.

Contact sensor systems offer some advantages, such as low cost, fast reaction speed, and high resistance to certain environmental factors. However, because such sensors can only detect and identify the crashes that have already happened, their triggering decisions may be available too late for some pedestrian protection systems. Moreover, contact sensors are always used to detect the impact on the bumper or the impact signal transferred though the bumper system. This will result in an unstable sensor output for the high temperature dependency of the bumper foam material.

1.6 Assessment of Pedestrian Protection

In order to assess the protective performance afforded by the car front for pedestrians in traffic accidents, European Enhanced Vehicle-safety Committee Working Group 17 (EEVC WG17) proposed impact tests for cars by using pedestrian subsystem impactors to represent the most frequently and seriously injured body parts (see Figure 1-9) (EEVC, 2002). The acceptance requirements of these tests are summarized in Table 1-7. These safety tests are already being used by the European New Car Assessment Program (EuroNCAP).

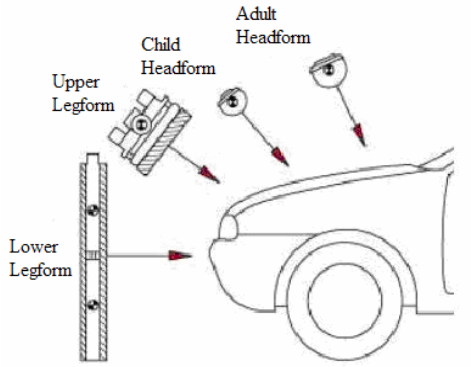

Figure 1-9 EEVC subsystem impact tests (EEVC, 2002)

Table 1-7 Acceptance requirements of the EEVC subsystem impact tests (EEVC, 2002)

Impact Test (40 km/h)	Acceptance Level	Injury Risk
Lower legform to bumper	Knee-bending angle ≤ 15°	-
	Knee-shearing displacement ≤ 6 mm	-
	Knee lateral acceleration ≤ 150 g	20% risk of AIS 2+
Upper legform to bonnet leading edge	Femur force ≤ 5 kN	20% risk of AIS 2+
	Femur-bending moment ≤ 300 Nm	
Child headform to bonnet top	$HIC_{15} \leq 1000$	-
Adult headform to bonnet top	$HIC_{15} \leq 1000$	20% of AIS 3+ (Mertz et al., 1996)

Based on the EEVC subsystem impact tests, the European Parliament and Council (2009) proposed two stages of subsystem impact tests with lower acceptance levels (see Table 1-8), which will be used on all cars in Europe.

Table 1-8 Subsystem impact tests proposed by European Parliament and Council (2009)

Date of Application	Test	Impact Speed	Acceptance Level
2009-11-24	Lower legform to bumper	40 km/h	Lateral knee-bending angle ≤ 21° Knee-shearing displacement ≤ 6 mm Knee lateral acceleration ≤ 200 g
	Upper legform to bumper	40 km/h	Instantaneous sum of femur force ≤ 7.5 kN Femur-bending moment ≤ 510 Nm
	Child headform to bonnet top	35 km/h	$HIC_{15} \leq 1000$ over 2/3 test area $HIC_{15} \leq 2000$ over 1/3 test area
2013-02-24	Lower legform to bumper	40 km/h	Lateral knee-bending angle ≤ 21° Knee-shearing displacement ≤ 6 mm Knee lateral acceleration ≤ 170 g
	Upper legform to bumper	40 km/h	Instantaneous sum of femur force ≤ 7.5 kN Femur-bending moment ≤ 510 Nm
	Child headform to bonnet top	35 km/h	$HIC_{15} \leq 1000$ on 1/2 child test area
	Adult headform to bonnet top	35 km/h	$HIC_{15} \leq 1000$ on 2/3 child/adult test area $HIC_{15} \leq 1700$ on other test area

2. METHODOLOGY

2.1 Mathematical Models

2.1.1 General

Mathematical models have played an increasingly important role in the analysis of crash accidents and the optimization of vehicle structures. Two methods are in wide use today.

- Multi Body System (MBS) Approach. An MBS is a system of rigid bodies connected by kinematic joints. These bodies usually have geometric shapes that often consist of ellipsoids. The joints constrain the relative motion between the connected bodies and thus reduce the system degrees of freedom. The motion of the bodies results from the equilibrium of applied forces and the rate of change in the momentum. This approach has demonstrated its advantage in modeling the responses of the whole body, such as the kinematics, force, and acceleration. However, this method is limited in the analysis of physical responses related to body deformation and contact between bodies. Typical MBS software includes MADYMO and PC-Crash.
- Finite Element (FE) Method. The FE method is a numerical technique used to find approximate solutions of partial differential equations and integral equations. Using this method, a complex solution domain is divided into a series of smaller regions (i.e., elements) in which the differential equations are solved approximately. By assembling the set of equations for each element, the behavior over the entire solution domain is determined. The process of dividing a domain into a finite number of elements is referred to as discretization. Elements are connected at specific points, called nodes. The assembly process requires the solution to be continuous along common boundaries of adjacent elements. The FE method can be implemented in a wide range of physical areas, such as thermal analysis, electromagnetic analysis, fluid dynamics, and structural analysis. For dynamic structural analysis, the FE method can be used to calculate not only the responses of the whole structure, but also those related to the deformation of the structure and the contact between structures. Compared to the MBS approach, the significant computational cost typically associated with the FE method represents a major limitation. Representative FE codes for dynamic structural analysis include LS_DYNA, RADIOSS, and PAM-CRASH.

In this study, the FE method was used to analyze the collisions between passenger cars and pedestrians. LS_DYNA was selected to conduct the simulations.

2.1.2 Fundamental Theory of Selected Software

LS_DYNA is a commercial FE code used to analyze the large deformation static and dynamic responses of structures. The primary solution methodology is based on explicit time integration. Figure 2-1 demonstrates a deformable body in a Cartesian coordinate system.

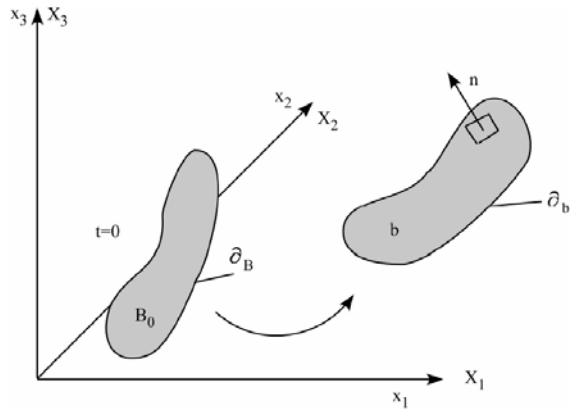

Figure 2-1 Deformable body in a Cartesian coordinate system (LSTC, 2006)

According to LSTC (2006), the current position of a point in the deformable body (see Figure 2-1) can be expressed as:

$$x_i = x_i(X_\alpha, t) \tag{2-1}$$

where x_i *(i=1, 2, 3)* is the current coordinates of the point, X_α *(α=1, 2, 3)* is the initial coordinates, and t is the time. At time *t=0*, the initial conditions can be written as:

$$x_i(X_\alpha, 0) = X_\alpha \tag{2-2}$$

$$\dot{x}_i(X_\alpha, 0) = V_i(X_\alpha) \tag{2-3}$$

where V_i is the initial velocities. The momentum equation of the point can be written as:

$$\sigma_{ij,j} + \rho f_i = \rho \ddot{x}_i \tag{2-4}$$

where $\sigma_{ij,j}$ is the Cauchy stress tensor, ρ is the current density, and the f_i is the body force density. The desired solution of the momentum equation will satisfy the traction boundary condition, the displacement boundary condition, and the contact discontinuity on the boundary ∂b_1, ∂b_2 and ∂b_3, respectively:

$$\sigma_{ij} n_j = l_i(t) \tag{2-5}$$

$$x_i(X_\alpha, t) = D_i(t) \tag{2-6}$$

$$\left(\sigma_{ij}^{+} - \sigma_{ij}^{-}\right) n_j = 0 \tag{2-7}$$

where σ_{ij} is the Cauchy stress, n_j is a unit outward normal to a boundary element of ∂b, $l_i(t)$ is the applied traction load, and $D_i(t)$ is the current displacement.

If Equation 2-4 is integrated with the current domain, the following expression can be obtained as:

$$\int_\Omega \left(\rho \ddot{x}_i - \sigma_{ij,j} - \rho f\right) \delta x_i d\Omega + \int_{\partial b_1} \left(\sigma_{ij} n_j - l_i\right) \delta x_i ds + \int_{\partial b_3} \left(\sigma_{ij}^{+} - \sigma_{ij}^{-}\right) n_j \delta x_i ds = 0 \tag{2-8}$$

where Ω is the current domain, and δx_i is an arbitrary displacement and satisfies the boundary condition on ∂b_2. If the divergence theorem is applied on Equation 2-8, the weak form of the equilibrium equation can be obtained as:

$$\int_\Omega \rho \ddot{x}_i \delta x_i d\Omega + \int_\Omega \sigma_{ij} \delta x_{i,j} d\Omega - \int_\Omega \rho f_i \delta x_i d\Omega - \int_{\partial b_1} l_i \delta x_i ds = 0 \tag{2-9}$$

If the domain is discretized by finite elements, the displacement of the point can be written as:

$$x_i(X_\alpha, t) = x_i(X_\alpha(\xi, \eta, \gamma), t) = \sum_{j=1}^{k} \phi_j(\xi, \eta, \gamma) x_i^j(t) \tag{2-10}$$

where ϕ_i is shape (interpolation) function of the parametric coordinates *(ξ, η, γ)*, k is the number of the nodes defining the element including the point, and x_i^j is the nodal coordinate of the j^{th} node in the i^{th} direction. In this case, Equation 2-9 can be expressed as:

$$\sum_{m=1}^{n} \left\{ \int_{\Omega_m} \rho \ddot{x}_i \Phi_i^m d\Omega + \int_{\Omega_m} \sigma_{ij}^m \Phi_{i,j}^m d\Omega - \int_{\Omega_m} \rho f_i \Phi_i^m d\Omega - \int_{\partial b_1} l_i \Phi_i^m ds \right\}^m = 0 \tag{2-11}$$

$$\Phi_i^m = \left(\phi_1, \phi_2, \cdots, \phi_k\right)_i^m \tag{2-12}$$

where n is the number of elements on the current domain. Equation 2-11 can be rewritten in matrix form as:

$$\sum_{m=1}^{n} \left\{ \int_{\Omega_m} \rho N^t N a d\Omega + \int_{\Omega_m} B^t \sigma d\Omega - \int_{\Omega_m} \rho N^t b d\Omega - \int_{\partial b_1} N^t l ds \right\}^m = 0 \tag{2-13}$$

where N is the interpolation matrix, σ is the stress vector, B is the strain-displacement matrix, a is the nodal acceleration vector, b is the body force load vector, and l is the applied traction load.

At time *I*, Equation 2-13 can be simply expressed as:

$$Ma^I = P^I - F^I \tag{2-14}$$

where *M* is the diagonal mass matrix, *P* is the external load vector, and *F* is the stress divergence vector. LS_DYNA uses the central difference method to update the time step to *I+1*:

$$a^I = M^{-1}\left(P^I - F^I\right) \tag{2-15}$$

$$v^{I+1/2} = v^{I-1/2} + a^I \Delta t^I \tag{2-16}$$

$$u^{I+1} = u^I + v^{I+1/2} \Delta t^{I+1/2} \tag{2-17}$$

$$\Delta t^{I+1/2} = \frac{\left(\Delta t^I + \Delta t^{I+1}\right)}{2} \tag{2-18}$$

$$x^{I+1} = x^0 + u^{I+1} \tag{2-19}$$

where *v* and *u* are the global nodal velocity and displacement vectors. The minimal time step Δt is decided by element size, material stiffness and density.

2.1.3 Biomechanical Material Laws

Various material laws are available in LS_DYNA for modeling human body tissues. In this section, the material laws commonly used for modeling human brain, ligaments and bones are introduced.

Viscoelastic Material: The viscoelastic material can be used to describe the viscoelastic property of soft tissues. It is commonly used for modeling the human brain in FE models. According to LSTC (2007), the shear relaxation behavior is described as:

$$G(t) = G_l + \left(G_s - G_l\right)e^{-\beta t} \tag{2-20}$$

where G_s is the short-term shear modulus, G_l is the long-term shear modulus, and β is the decay constant.

Material of Strain-Rate Dependent Plasticity: The material law of strain-rate dependent plasticity describes that the material yield strength changes with the effective strain rate. It can be used for modeling human ligaments in FE models. According to LSTC (2007), the yield stress σ_y can be defined as:

$$\sigma_y = \sigma_0\left(\dot{\varepsilon}\right) + E_p \varepsilon_p \tag{2-21}$$

where σ_0 is the yield strength which is a function of the effective strain rate $\dot{\varepsilon}$, ε_p is effective plastic strain, and E_p is defined as:

$$E_p = \frac{EE_t}{E - E_t} \tag{2-22}$$

where *E* is the Young's modulus, and E_t is the tangent modulus.

Material of Simplified Johnson-Cook: The material of simplified Johnson-Cook is used in problems where the strain rate varies over a wide range. It can be used for modeling human bones in FE models. According to LSTC (2007), the yield stress σ_y can be defined as:

$$\sigma_y = \left(A + B\varepsilon_p^n\right)\left(1 + C\ln\dot{\varepsilon}\right) \tag{2-23}$$

where *A*, *B*, *C*, and *n* are input constants.

2.1.4 Human Body FE Models

Since the 1990s, a number of human body FE models have been developed to analyze human injury mechanisms in traffic crashes. These models include fully-body models and models of various body parts.

Full-body FE models have been developed to analyze the responses of the full human body to traffic collisions. Huang et al. (1994) developed a full-body model to predict the responses of car occupants during side impacts. In this model, only the rib cage was represented in detail; the other body parts were simplified. The model was validated based on cadaver (occupant) side impacts and lateral pendulum impacts. This simplified model was found to be effective in estimating chest injury parameters and evaluating car structures for side impact protection. Maeno and Hasegawa (2001) and Iwamoto et al. (2002) presented a detailed full-body human model to study the injury mechanisms of car occupants and pedestrians. This model was named Total HUman Model for Safety (THUMS) and was validated against a cadaver (pedestrian) side impact, cadaver (pedestrian) pelvis and lower limb impacts, and cadaver (occupant) body segment impacts. This study concluded that the THUMS model was a promising tool for reconstructing multiple human injuries in traffic crashes. Robin (2001) presented a detailed full-body model, named HUman Model for safety (HUMOS), to study the injury mechanisms of car occupants. The separate body parts of the HUMOS model were validated against the corresponding body segment impacts, respectively. Following the work of Robin (2001), Vezin and Verriest (2005) presented a group of full-body models (HUMOS2) to study the injury mechanisms of car occupants and pedestrians. In this study, a 5th percentile female occupant model, a 50th percentile male occupant model, and a 95th percentile male pedestrian model were scaled from the HUMOS model and refined for important body parts. These models were again validated based on cadaver (occupant) front and oblique impacts. Additional full-body models can be found in published literature, and some of the published models are introduced in Table 2-1.

Table 2-1 Full-body FE models

Resource	Size	Elements	Posture	Validation
Huang et al., 1994	50th percentile male	About 12,000	Seating	Side impacts Lateral pendulum impacts
Lizee et al., 1998	50th percentile male	About 10,000	Seating	30 test configurations
Maeno and Hasegawa, 2001 & Iwamoto et al., 2002	50th percentile male	About 83,000	Seating & standing	Pedestrian lower limb impacts Pedestrian pelvis side impacts Pedestrian side impact Body segment impacts
Robin, 2001	50th percentile male	About 50,000	Seating	Body segment impacts
Ruan et al., 2003	50th percentile male	About 119,000	Seating	Frontal pendulum impacts Side pendulum impacts Belt loading
Vezin and Verriest (2005)	5th percentile female 50th percentile male 95th percentile male	-	Seating Seating Standing	Front impacts Oblique impacts
Kimpara et al., 2005	5th percentile female	About 116,000	Seating	Frontal pendulum impacts Side pendulum impact Oblique pendulum impacts Ballistic best impact

Lower limb FE models are used to analyze the injury mechanisms of human lower limbs in collisions with vehicle structures. Iwamoto et al. (2000) developed a detailed lower limb FE model to predict the lower extremity injuries of car occupants in full front and offset front impacts. This model was validated against three-point bending tests for long bones, quasi-static bending tests for ankle joints and the impact test on the foot region. It was concluded that the fractures of the bones of the ankle/foot region can be predicted by this model. Beillas et al. (2001) developed a human Lower Limb Model for Safety (LLMS). This model represented the detailed anatomical structures of the lower limb of a 50th percentile male. It was validated globally for some of the common injury mechanisms encountered in both frontal and pedestrian impacts. This study concluded that the model was able to simulate both kinematic and deformable behaviors simultaneously. Nagasaka et al. (2003) presented a detailed lower limb model to assess injuries to the lower extremities of a pedestrian. The model was derived from the THUMS model and refined further for lower limb impacts. Cadaver knee shearing and bending tests were used to validate this model. Huang et al. (2008) developed a lower limb model to study the injuries of pedestrian lower extremities in car collisions. This model was derived from the HUMOS2 model and refined for lower limb collisions. Cadaver knee shearing and bending tests were used to validate this model. This study identified that the lower limb model can simulate the kinematics and injuries of pedestrians' lower extremities in car collisions. Additional lower limb models appear in published literature, and Table 2-2 summarizes some of the published models.

Table 2-2 Human lower limb FE models

Reference	Size	Elements	Posture	Validation
Iwamoto et al., 2000	50th percentile male	-	Seating	Three-point bending tests for long bones Quasi-static bending tests for ankle joint Impact test on the foot region
Schuster et al., 2000	-	-	Standing	Three-point bending tests for long bones Shearing and bending tests for knee
Beillas et al., 2001	50th percentile male	25,000	Seating	Static axial compression tests along tibia Horizontal impacts on patella Vertical impacts on tibia Shearing tests on tibia Shearing and bending tests for knee
Nagasaka et al., 2003	50th percentile male	-	Standing	Shearing and bending tests for knee
Takahashi et al., 2003	50th percentile male	-	Standing	Three-point bending tests for long bones Quasi-static tensile tests for ligaments Dynamic tensile tests for ligaments Shearing and bending tests for knee
Rooij et al., 2004	50th percentile male	-	Seating	Knee-femur response tests Knee-thigh-hip tolerance tests
Untaroiu et al., 2005	50th percentile male	18,500	Standing	Three-point bending tests for long bones Compression tests for lower limb Three-point bending tests for leg Three- and four-point knee bending tests
Kikuchi et al., 2006	50th percentile male	-	Standing	Three-point bending tests for thigh and leg Tensile tests for knee ligaments Four-point bending tests for knee
Huang et al. 2008	50th percentile male	16.945	Standing	Shearing and bending tests for knee

Head FE models are used to analyze the injury mechanisms of the human head in collisions with vehicle structures. Zhou et al. (1995) presented a human head model to represent the detailed anatomical structures of the head of a 50th percentile male. It was validated against a cadaver head frontal impact test. Kang et al. (1997) presented a detailed human head model to reconstruct the head impact caused by a motorcycle accident. This model was named the head model of Universite Louis Pasteur (ULP) and was validated based on cadaver head frontal impact. The results of this study proved the good performance of the UPL model to predict the site of brain injury. Zhang et al. (2001) developed a human head model to simulate direct and indirect impacts over a wide range of severities. This model was named the Wayne State University Brain Injury Model (WSUBIM). It was validated against a number of cadaver head frontal, occipital, and facial impacts. Further, the WSUBIM model can be considered as a powerful tool with which to understand further the injury mechanisms and the tolerances of the brain to blunt impacts. Yang et al. (2008) developed a human head model to analyze the collisions between the pedestrian head and the car hood. This model represented all essential anatomical features of a 50th percentile male head and was validated against cadaver head frontal and facial impacts. It was identified as a promising tool with which to understand the injury mechanisms of the brain in blunt impacts. Information about additional head models has been published in recent years, and some of the published models are summarized in Table 2-3.

Table 2-3 Human head FE models

Reference	Size	Elements	Validation
Zhou et al., 1995	50th percentile male	22,995	Frontal impact
Ruan et al., 1996	-	9,146	Frontal impact
Turquier et al., 1996	-	5,400	Forehead and face impacts
Kang et al., 1997	-	13,208	Frontal impact
Zhang et al., 2001	50th percentile male	314,500	Frontal and occipital impacts Facial impacts
Kleiven and Hardy, 2002	-	18,416	Frontal and side impacts
Takhounts et al., 2003	50th percentile male	7,852	Frontal, occipital and temporal impacts
Deck et al., 2004	-	74,243	Frontal shock Vertex and occipital impacts
Ejima et al., 2004	Small male	1,220,000	Frontal impact
Yao et al., 2008	-	-	Frontal impact
Takhounts et al., 2008	50th percentile male	45,875	Frontal, occipital and temporal impacts
Yang et al., 2008	50th percentile male	61,121	Frontal and facial impacts

2.2 Statistical Methods of Experiment Design

The statistical method of factorial experiment design was used to investigate the effects of the design parameters of the RBS and the RH on pedestrian responses in car collisions. The response surface method was implemented to optimize the design configurations of the RH for the head protection of adult pedestrians.

2.2.1 Method of Factorial Experiment Design

Box et al. (2005) presented the statistical method to calculate and evaluate the effects of experimental factors on experimental results. According to this method, the effects of the design parameters of the RBS and the RH can be calculated as:

$$Eff = \frac{1}{m}\sum_{i=1}^{m} R_{+i} - \frac{1}{n}\sum_{j=1}^{n} R_{-j} \qquad 2\text{-}24$$

where *Eff* is the effect of some design parameter, R_{+i} is the simulation result for one value of the parameter with m being the number of the results, and R_{-j} is the result for another value of the parameter with n being the number. Because the FE method was used to analyze the car-pedestrian collisions in this study, the repeat measurements of the simulation results were unfeasible. Therefore, the variance of the effect was estimated by:

$$S^2_{Eff} = \frac{\sum_{i=1}^{m}(R_{+i} - R_{+})^2 + \sum_{j=1}^{n}(R_{-j} - R_{-})^2}{m+n-2} \qquad 2\text{-}25$$

where S_{Eff} is the estimated variance of the effect, R_{+} is the average result for one value of the design parameter, and R_{-} is the average result for another value of the parameter. The null hypothesis was presented as the effect being zero. The *P*-value of the effect was thus calculated as:

$$P = t\left(\frac{Diff - 0}{S_{diff} \times \sqrt{\frac{1}{m} + \frac{1}{n}}}, m+n-2, 1\right) \qquad 2\text{-}26$$

where t is the Student's t distribution and $m+n-2$ gives the degrees of freedom, and 1 means the *P*-value is one-tail *P*-value. Where the *P*-value is less than 0.05, the null hypothesis should be statistically refused and the effect is significant.

2.2.2 Response Surface Method

Box et al. (2005) presented the response surface method to explore the relationship between experimental factors and the result. According to this method, the response surfaces expressed by polynomials were developed to represent the relationship between the design variables of the RH and the impact responses of pedestrian heads. A response surface can be written in matrix form as:

$$Y = X \times B \qquad 2\text{-}27$$

where Y is the response vector, X is the matrix of the design variables, and B is the constant coefficient vector. The B vector can be solved using the least square method as:

$$B = (X^T \times X)^{-1} \times X^T \times Y \qquad 2\text{-}28$$

Thus, the response surface was obtained. For the developed response surface, the sum of squared residuals (*SSR*) was calculated by:

$$SSR = (Y - X \times B)^T \times (Y - X \times B) \qquad 2\text{-}29$$

For each response surface, the order of the polynomial was selected to minimize the *SSR*.

In order to assess the accuracy of the response surface, extra experiments should be conducted. The results obtained from such extra experiments and predicted by the response surface can be compared as:

$$APE = \sqrt{\frac{\sum_{i=1}^{s}(y_i - y_i')^2}{s}} \qquad 2\text{-}30$$

where APE is the average prediction error, y_i is the response obtained from the simulation, y_i' is the response predicted by the response surface, and s is the number of the simulations. Then, the Lack Of Fit (LOF) test should be conducted to estimate the statistical significance of APE. If APE is significant, the response surface is not sufficiently accurate; otherwise, the response surface can be accepted. In this study, the FE method was used instead of physical tests to analyze car-pedestrian impacts. As a result, the LOF test cannot be conducted to estimate the significance of APE. However, APE can still provide a general indication on the accuracy of the response surface.

3. AIM OF STUDY

The overall aim of this study is to evaluate and optimize the performance of the integrated safety system. The specific goals of this study include:

- An evaluation of the effectiveness of the remote sensor system in detecting pedestrians at risk in a vehicle traffic environment;
- An analysis of the performance of the contact sensor for the temperature-independent measurement of pedestrian impacts;
- An investigation into the efficiency of the RBS, in different design configurations and various impact conditions, in protecting pedestrians' lower limbs; and,
- Evaluation and optimization of the RH performance relative to the prevention of head injuries among adult pedestrians due to hood collisions.

4. SUMMARIES OF PAPERS I-IV

4.1 Paper I

Evaluation of Remote Pedestrian Sensor System Based on the Analysis of Car-Pedestrian Accident Scenarios

Objectives: This study evaluated the effectiveness of a remote sensor system for detecting pedestrians at risk in a vehicle traffic environment.

Methods: The main data source for this study was the STRADA database. As described in Table 4-1, nine scenarios of car-pedestrian accidents were defined in STRADA according to pedestrian and car trajectories, and accident locations. From January 1, 1999, to September 13, 2005, 2,199 car-pedestrian impacts with identified accident scenarios were recorded in the database. These cases were selected and analyzed further in the current study. Based on this analysis, the two most common scenarios were identified. Subsequently, the qualitative and quantitative knowledge indicated in Table 4-2 was developed for these two scenarios. The qualitative pedestrian and car trajectories were obtained from the definition of the accident scenarios, while the quantitative speeds of pedestrians and cars were estimated statistically. Based on the qualitative and quantitative knowledge developed, a mathematical model was presented from the hypothesis that all pedestrians in the detection range of the sensor system will be detected in a timely manner. The remote sensor system was then evaluated using this model.

Table 4-1 Description of the accident scenarios

Scenario	Description
F1	Pedestrian crossing road, car coming from the left side of the pedestrian
F2	Pedestrian crossing road, car coming from the right side of the pedestrian
F3	Pedestrian moving along the left side of road
F4	Pedestrian moving along the right side of road
F5	***Pedestrian crossing before intersection, car going straight forward***
F6	***Pedestrian crossing after intersection, car going straight forward***
F7	Pedestrian crossing after intersection, car turning left
F8	Pedestrian crossing after intersection, car turning right
F9	Pedestrian standing in the path of the oncoming vehicle

Table 4-2 Variables for car-pedestrian accident scenarios

	Variable
Qualitative Knowledge	Trajectory of pedestrian
	Trajectory of car
Quantitative Knowledge	Speed of pedestrian
	Velocity of car
	Location of impact point on car

Results: It was identified that F6 was the most common scenario and accounted for 683 car-pedestrian accidents (31.1%) among the 2,199 cases selected. F5 was the second most common scenario and accounted for 347 car-pedestrian impacts (15.7%) of the 2,199 accidents. Because F5 and F6 were the two most common accident scenarios, the qualitative and quantitative knowledge was developed exclusively for them.

According to the description of accident scenarios F5 and F6 in Table 4-1, the moving trajectories of the pedestrians and cars were directly obtained. In these two scenarios, the moving trajectories of the pedestrians and passenger cars are straight, meeting at a 90-degree angle. Based on the pedestrians' ages, the road speed limits at accident locations, and the damages to cars, the pedestrian speeds, the car velocities, and the locations of the impact points on cars were estimated. A mathematical model (Figure 4-1) was developed to evaluate the effectiveness of the sensor system in accident scenarios F5 and F6.

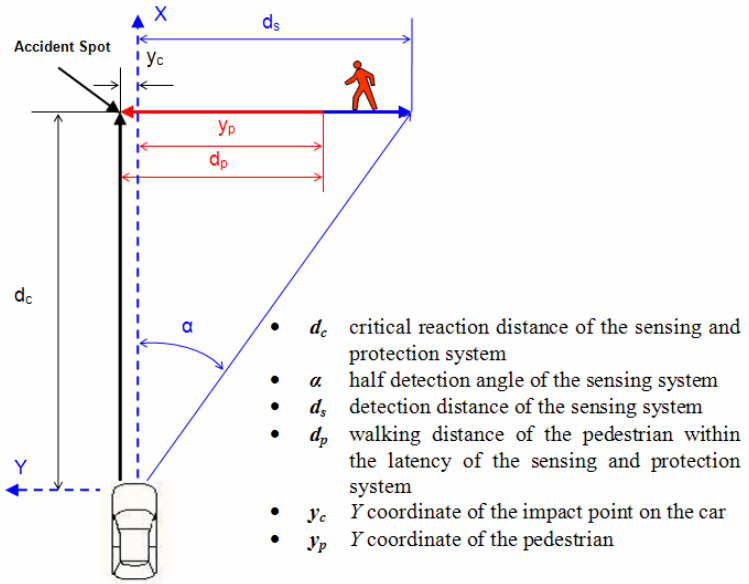

Figure 4-1 Mathematical model for the evaluation of the sensor system

For any case covered by this model, d_c can be calculated using:

$$d_c = v_c \times t_r \qquad 4\text{-}1$$

where v_c is the car velocity and t_r is the latency of the sensor and protective system. In addition, d_p can be calculated using:

$$d_p = v_p \times t_r \qquad 4\text{-}2$$

where v_p is the pedestrian speed. Thus, d_s and y_p can be obtained from:

$$d_s = d_c \times \tan(\alpha) \qquad 4\text{-}3$$

$$y_p = d_p - y_c \qquad 4\text{-}4$$

If y_p is smaller than d_s, the sensor system can detect the pedestrian in a timely manner.

If the effectiveness of the sensor system is evaluated in the entire accident scenario, the probability density functions of car velocities, pedestrian speeds, and Y coordinate values of impact points can be used in Equations 4-1, 4-2, and 4-4 as V_c, V_p and Y_c. According to Equations 4-3 and 4-4, D_s and Y_p become random variables as well. The effectiveness of the sensor system for pedestrian detection can therefore be calculated using:

$$P = 1 - \int_0^{\infty} Y_p(x) \int_0^{x} D_s(y) dy dx \qquad 4\text{-}5$$

where P is the probability of the pedestrian being detected in time and $Y_p(x)$ and $D_s(y)$ are the probability density functions of Y_p and D_s, respectively. Using this model, the probabilities for pedestrians being detected in the F5 and F6 scenarios were calculated in terms of the different detection angles (Table 4-3).

Table 4-3 Probability of pedestrians being detected in a timely manner

Detection Angle	Accident Scenario	*Probability*	
		Pedestrian Walking	Pedestrian Running
45°	F5	1.000	1.000
	F6	1.000	1.000
30°	F5	1.000	0.998
	F6	1.000	0.997
15°	F5	0.991	0.734
	F6	0.987	0.657

Discussion: Based on the analysis of the pedestrian accidents recorded in the STRADA database, the two most common scenarios for the pedestrian accidents in Sweden were identified as cars entering and leaving intersections and colliding with pedestrians crossing the road. According to the definitions of the scenarios, the trajectories of the pedestrians and cars were obtained as moving straight forward and meeting at a 90-degree angle. The speeds of pedestrians, velocities of cars, and locations of the impact points on cars were estimated statistically for these two scenarios.

Based on the knowledge developed, the mathematical model was designed to evaluate the effectiveness of the sensor system in the accident scenarios. This evaluation identified that in order to detect all pedestrians in the two scenarios in a timely manner, the detection angle of the sensor system must be greater than 60°.

4.2 Paper II

Performance Analysis of a Bumper-Pedestrian Contact Sensor System Using FE Models

A bumper-pedestrian contact sensor was developed to detect impacts with pedestrians and trigger pedestrian protective systems (e.g., a RH). The main component of the contact sensor was a sealed air tube within bumper foam. As the environmental temperature increased, the bumper foam around the tube softened while the air tube stiffened due to its higher pressure. Similarly, when the environmental temperature decreased, the bumper foam stiffened while the air tube softened. In this way, the temperature-dependent change in bumper foam stiffness was compensated by the opposite change in the stiffness of the air tube, enabling the sensor output—the change of the air pressure in the tube—to remain relatively stable.

Objective: This study intended to analyze the performance of the contact sensor for the temperature-independent measurement of pedestrian impacts.

Methods: A baseline bumper FE model was developed and validated using EuroNCAP lower legform impact tests performed on the production bumper. Based on this baseline model, an improved bumper model was developed to meet the requirements of EEVC WG17 lower legform impact tests. An FE lower limb model was then derived from the HUMOS2 full human body model. Using this lower limb model, the protective performance of the baseline and improved bumper models was evaluated further. Finally, the contact sensor was built into the improved bumper model (see Figure 4-2). Two different sensor tubes of 25 and 50 mm in diameter were compared in the simulations. At each temperature (i.e., -30, 20 and 85 degrees Celsius) the improved bumper model, with its integrated sensor tube, was impacted by both the EEVC lower legform model and a 1 kg impactor model on the bumper central line. Consequently, a better diameter of the sensor tube was identified in terms of the temperature stability and mass sensitivity of the sensor output.

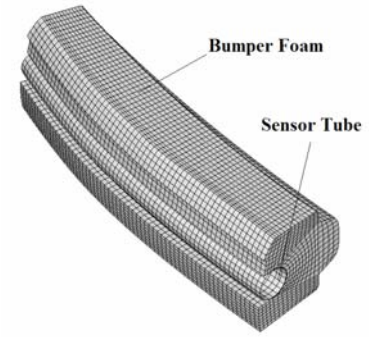

Figure 4-2 Half-bumper foam model integrating the sensor tube

Results: The legform responses obtained from the EuroNCAP tests performed on the production bumper and the corresponding simulations were comparable. The baseline bumper model was valid. Based on the valid baseline bumper model, the improved bumper model was developed to achieve enhanced protective performance for pedestrians' lower limbs. It was determined that the improved bumper model can meet the acceptance requirements of EEVC WG17. The human lower limb model was used to compare further the protective performance of the baseline and improved bumper models, determining eventually that the improved bumper model protected the knee joint more efficiently. However, because of the stronger lower stiffener used in the improved bumper model, the risk for tibia and fibula fractures increased.

Figure 4-3 compares the sensor outputs from the impacts with two objects of different mass at -30, 20, and 85 degrees Celsius. Table 4-4 summarizes the peak values of the sensor outputs. With the 50 mm sensor tube implemented, the minimum difference between the peak values of the sensor outputs during the impacts with the two objects was 14.9 kPa. During the collisions with the 1 kg impactor, the maximum difference between the peak values was 0.8 kPa. During the impacts with the EEVC legform, the maximum difference was 6 kPa. When the 25 mm sensor tube was implemented, the minimum difference between the peak values of the sensor outputs during the impacts with the two objects was 17.2 kPa. In the collisions with the 1 kg impactor, the maximum difference in the peak values was 2 kPa, while during the impacts with the EEVC legform, this difference was 1.8 kPa.

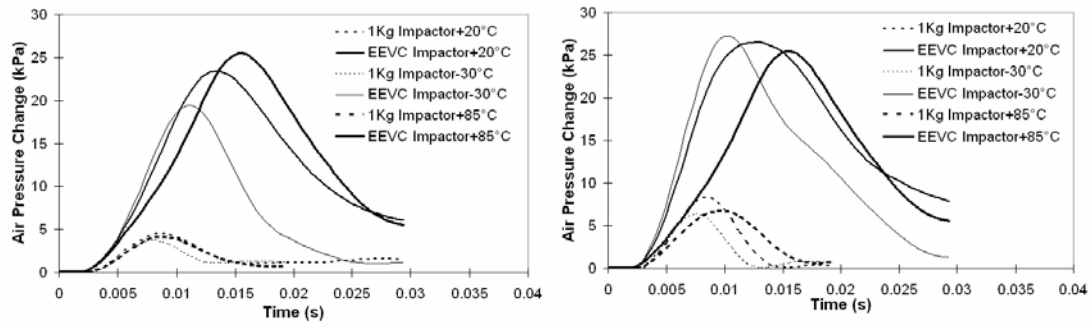

(a) 50 mm sensor tube **(b) 25 mm sensor tube**

Figure 4-3 Comparison of sensor outputs

Table 4-4 Maximum air pressure change in the 50 mm sensor tube

Impactor	Sensor Tube	Maximum Air Pressure Change (kPa)		
		-30°C	20°C	85°C
1-kg Impactor	50 mm	3.7	4.5	4.1
	25 mm	6.3	8.3	6.7
EEVC Legform	50mm	19.4	23.4	25.4
	25 mm	27.3	26.5	25.5

Discussion: The baseline bumper model failed to meet the acceptance requirements of the EEVC WG17 lower legform tests. By improving the bumper design, however, the protective performance of the bumper model was enhanced to the level that the virtual testing results met the EEVC requirements. The protective performance of the baseline and improved bumper models was further evaluated and confirmed using the human lower limb model. The improved bumper model was found to protect the human knee joint more efficiently, while the risk for tibia and fibula fractures increased. Considering the comprehensive effect of the improved bumper design, a more effective lower limb protection can be achieved.

Enhanced sensor output stability and mass sensitivity can be achieved by optimizing the diameter of the sensor tube. When using a 25 mm rather than 50 mm sensor tube, the sensor output was more stable at varying temperatures in the EEVC WG17 legform impacts and more sensitive to the different masses of the impact objects. Therefore, the 25 mm sensor tube was a better choice for the design of the bumper contact sensor.

4.3 Paper III

A Reversible Bumper System for Protecting Pedestrian Lower Limbs from Car Collisions

Objective: In order to improve the protective performance of an RBS, this study investigated the efficiency of the RBS of different design configurations in various impact conditions.

Methods: In this study, the protective performance of the RBS was investigated using FE modeling of legform impactor collisions and human lower limb impacts. A car front FE model was developed and validated based on the EuroNCAP lower legform impact tests performed on the production car front. An RBS model (see Figure 4-4) was subsequently developed based on the original bumper in the car front model. In order to investigate the protective performance of the RBS, the pedestrian lower limb FE model and the EEVC WG17 lower legform FE model were used to collide with the RBS model of different design configurations under various impact conditions (see Table 4-5). Finally, the effects of the design configurations on the protective performance of the RBS were calculated using the statistical method of the factorial experiment design.

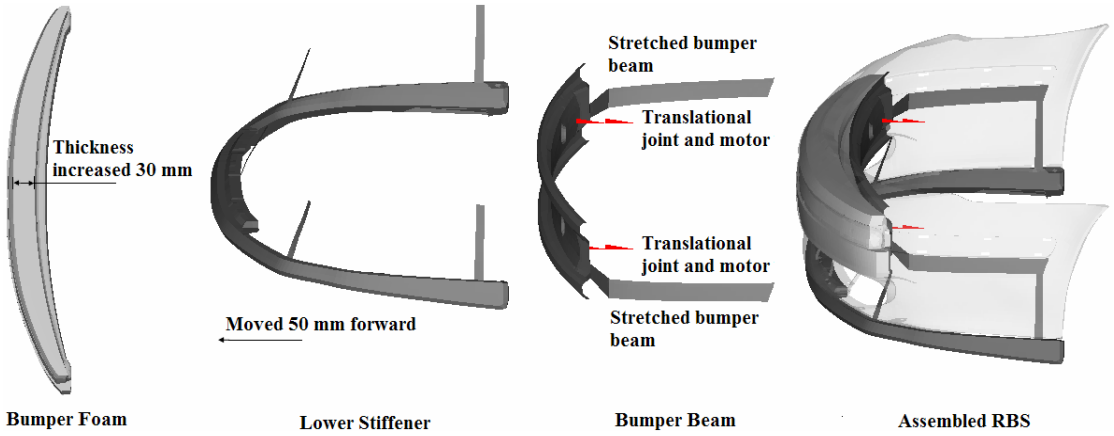

Figure 4-4 RBS FE model

Table 4-5 Design configurations and impact conditions for the RBS

Bumper Stiffness		Bumper Deploying Speed	Max. Deployment Distance	Deployed Distance
Bumper Foam	Lower Stiffener	(m/s)	(mm)	(mm)
80 g/l EPP	3 mm steel	0	0	0
30 g/l EPP	1 mm steel	2.5	100	50
-	-	5	150	75
-	-	-	-	100
-	-	-	-	150

The deployed distance is the extended distance of the bumper at the initiation of impact. If the deployed distance is equal to the maximum deployment distance, the RBS model is static and rigidly fixed. The bumper deploying speed is 0 m/s. If the deployed distance is equal to half of the maximum deployment distance, the RBS model extends at a constant deploying speed.

Results: The legform responses obtained from the EuroNCAP tests performed on the car front and the corresponding simulations were comparable. The car front model was valid.

The responses of the legform model and the human lower limb model during the impacts with the RBS model were compared. When the same bumper design configuration and impact condition were presented, the peak tibia accelerations of the standard EEVC legform model and the human lower limb model were comparable. However, the peak knee-bending angle of the lower limb model was more than twice that of the legform model. When the bumper stiffness was at the higher level, the peak knee-shearing displacement of the lower limb model was more than twice that of the legform model. Furthermore, when the bumper stiffness was at the lower level, the lower limb model had a peak knee-shearing displacement that was five to seven times higher than the legform model.

The main effects of bumper stiffness on the responses of the legform model and human lower limb model were significant. When the bumper stiffness was at the lower level, the average peak tibia acceleration was reduced by 106.4 g for the legform model and 72.3 g for the lower limb model. The mean value of the peak knee-shearing displacements was reduced by 2.8 mm for the legform model but increased by 3.0 mm for the lower limb model. Furthermore, the average peak knee-bending angle was reduced by 7 degrees for

the legform model and 19.3 degrees for the lower limb model. The average number of the injuries predicted by the lower limb model was reduced by 1.3.

When the bumper deploying speed changed from 0 to 2.5 m/s, the main effects relative to the responses of the lower limb model were significant. Colliding with the RBS model that was deploying at a speed of 2.5 m/s increased the average peak tibia acceleration of the lower limb model by 51.8 g, the mean value of the peak knee-shearing displacement by 2.8 mm, the average peak knee-bending angle by 16.4 degrees, and the average number of lower limb injuries by 1.4. Concerning the responses of the legform model, the only significant main effect was that of the knee-bending angle. Colliding with the bumper model that was deploying at a speed of 2.5 m/s increased the average peak knee-bending angle of the legform model by 6.4 degrees. When the bumper deploying speed increased from 2.5 m/s to 5 m/s, the main effects were not significant. The protective performance of the RBS did not result in any obvious changes.

When the maximum deployment distance of the RBS model was less than 150 mm, the main effects of this parameter were not significant. In this case, the protective performance of the fully deployed bumper was the same as the retracted bumper.

Discussion: The bio-fidelity of the EEVC WG17 lower legform impactor was poor for the knee kinematics. It is doubtful that the legform impactor can be used to predict pedestrians' knee injuries accurately.

The performance of the RBS for protecting pedestrians' lower limbs can obviously be improved by reducing the bumper stiffness. However, its performance was impaired when deploying at a speed of 2.5 m/s or greater. Less than 150 mm, the maximum deployment distance of the specific RBS had no influence on the bumper protective performance. Thus, the deployment of the specific RBS cannot contribute directly to the protection of pedestrians' lower limbs.

The calculated injury parameters from the human lower limb FE model can be used for the evaluation of the protective performance of a newly designed bumper system.

4.4 Paper IV

Optimization of a Reversible Hood for Protecting a Pedestrian's Head during Car Collisions

Objective: The current study evaluated and optimized the performance of the RH for the prevention of head injuries among adult pedestrians due to hood collisions.

Methods: A car front FE model was developed and validated based on the EuroNCAP adult headform impact tests conducted on the car hood. The baseline RH was subsequently developed from the original hood in the validated car front model (see Figure 4-5). In order to evaluate the protective performance of the baseline RH, the FE models of a 50th percentile human head and the EEVC WG17 adult headform were used in parallel to impact the baseline RH in the lifting states defined in Table 4-6. This was accomplished by repeating the impact configurations of the EuroNCAP adult headform tests (see Figure 4-5). In order to minimize the HIC values of the headform model, the response surface method was applied to optimize the RH in terms of material stiffness, lifting speed, and lifted height. Finally, the headform and human head models were used again to evaluate the protective performance of the optimized RH.

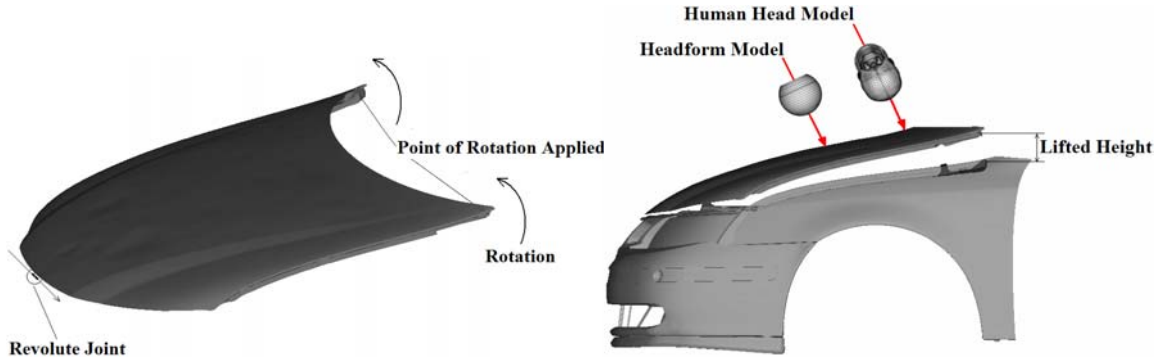

Figure 4-5 Baseline RH and evaluation

Table 4-6 Lifting states of the RH

State	Definition
A	The hood was static in the fully retracted position.
B	The rear end of the hood had lifted 53 mm and was continuing to rise.
C	The hood was static in the fully lifted position.

Results: The headform HIC values obtained from the EuroNCAP adult headform tests and the corresponding simulations were comparable except at a few impact points. The car front model was valid.

The impact responses of the headform and human head models in collisions with the baseline RH achieved the lowest levels in state C. Comparison of the impact responses between states B and C indicated that the lifting speed of the baseline RH can increase the impact responses of the headform and human head models. The pedestrian's head can be protected better in state C than in state B. Comparison of the impact responses between states C and A disclosed that the lifted rear of the baseline RH can reduce impact responses except for the angular acceleration of the human head model. The pedestrian's head can be protected better in state C than in state A. Using the HIC values of the headform and human head models, pedestrian fatality risks were compared between states A and C. Pedestrian fatality risks were demonstrably reduced in state C compared to state A.

In order to minimize the mean HIC values of the headform model in states A, B, and C, the optimized material stiffness was ultimately determined to be 71 GPa. The optimized lifting speed was 2.2 rad/s while the optimized lifted height was 214 mm. The impact responses of the headform and human head models in collisions with the optimized RH were also obtained. Impacts with the optimized RH in state C resulted in lower HIC values of the headform and human head models than the EEVC limit of 1,000.

The impact responses were compared between the baseline and the optimized RH. Since the optimized material stiffness of the RH was the same as the stiffness used in the baseline RH, no difference existed between the baseline and the optimized RH in state A. Consequently, the same impact responses were obtained from the collisions with the baseline and the optimized RH in state A. In states B and C, the angular acceleration of the human head model can be reduced by implementing of the optimized RH. The

remaining impact responses of the headform and human head models were also reduced. However, the reduction of these responses was not statistically significant.

The HIC values of the headform model as well as the HIC values and intracranial pressures of the human head model were compared during the evaluation of the optimized RH. Except at certain impact points, the HIC values of the headform model coincided well with the HIC values of the human head model. The change in the intracranial pressure of the human head model can predict the change of the HIC values of the headform and human head models.

Discussion: When compared with the retracted baseline RH (in state A) and the lifting baseline RH (in state B), the lifted baseline RH (in state C) can reduce the impact responses of the headform and human head models. Compared to the retracted baseline RH (in state A), the lifted baseline RH (in state C) can reduce the risk of pedestrian fatality from head impacts.

In states B and C, further reduction of the impact responses of the headform and human head models can be realized through implementation of the optimized rather than the baseline RH. When the optimized RH was lifted (in state C), the HIC values of the headform and human head models were reduced further, falling much lower than 1,000. Thus, the risk of pedestrian head injuries can be minimized as required by EEVC WG17.

Under the same impact conditions, the HIC value of the human head model coincided with that of the headform model. The change in the intracranial pressure of the human head model can predict the change in the HIC values of the headform and human head models.

5. GENERAL DISCUSSION

Although pedestrian safety has improved in highly motorized countries, pedestrian casualties remain prominent in traffic accidents. As discussed herein, passenger cars are overrepresented in pedestrian traffic accidents. Moreover, the car front is the major contact source in pedestrian crashes. Several systems were developed to protect pedestrians from collisions with the car front. In order to trigger these pedestrian protective systems, different sensor systems were presented to detect pedestrian impacts. It is important to evaluate and improve the performance of the pedestrian sensor and protective systems.

This study contributed to the evaluation and optimization of the performance of an integrated pedestrian safety system. Papers I and II evaluated the performance of a remote sensor system and a contact sensor for the detection of pedestrian impacts, while Papers III and IV evaluated and optimized the performance of an RBS and an RH to protect pedestrians during car collisions.

5.1 Collection of Accident Data

The accident data investigated in Paper I were extracted from the STRADA database. This source has been developed by SRA since 1996 to store the road accident data collected from the police and hospitals. Since January 1, 2003, all police stations and approximately 50% of the emergency hospitals in Sweden have reported traffic accident data to STRADA.

For each event in the STRADA database, the police are responsible for providing information from the scene of the accident, including a description of the accident environment and classification of the accident scenario. However, only simple information about the human injuries sustained in the accident is available in the police report. Instead, emergency hospitals provide detailed records of the human injuries and their scales. All accidents reported by the police and hospitals are coded respectively. By using a unique identity number, a police case can be linked with its corresponding record from hospitals. However, for most of the pedestrian accidents in the database, this linkage is ineffective and results in incomplete information on many accidents. Consequently, comprehensive research that requires information from both the police and hospitals becomes difficult.

Generally, information about pedestrian movement is recorded in accident databases in terms of different gaits, such as walking, trotting, or running. Based on this information, pedestrian speed in traffic accidents can be estimated accurately. In the STRADA database, however, the information on pedestrian movement is not recorded at all. In fact, not only is pedestrian speed missing, but also their gaits. As a result, estimating pedestrian speed becomes difficult, and several hypotheses must be used, as described in Paper I. Moreover, the STRADA database does not record information about vehicle velocity. With no other option available, the vehicle velocities used in Paper I were estimated based on the speed limits in effect at accident locations.

Not only is the STRADA database missing pedestrian speed and vehicle velocity, but some other critical information as well. For example, in many car-pedestrian accidents, the cars braked before collision. Since this factor is not recorded in the database, it was not considered in the mathematical model developed in Paper I. Consequently, the performance of the remote sensor system may be overestimated. If a pedestrian is obstructed, the effectiveness of the sensor system can still be calculated using a minimally alerted mathematical model. However, the pedestrian visibility is not recorded in STRADA either, so it is not considered in Paper I. As a result, the performance of the sensor system may once again be overrated.

5.2 Classification of Accident Scenarios

Following the original pedestrian accident typology developed in NHTSA (Snyder and Knoblauch, 1971; Knoblauch and Knoblauch, 1976), many accident taxonomies were developed to understand pedestrian accidents better. Schofer et al. (1995) presented a simple four-category taxonomy of child pedestrian-motor vehicle accidents based on the process that led to the collision. This structure has been recognized as being useful for identifying and organizing interventions. In order to describe the relationship between the various factors involved in fatal pedestrian accidents, Fontaine and Gourlet (1997) proposed a typology of fatal pedestrian accidents based on cases in France from March 1990 to February 1991 and identified four overrepresented pedestrian groups. Meanwhile, in order to analyze the influence of

supervision in child pedestrian accidents, Wills et al. (1997) presented a classification of child pedestrian accidents according to 10 patterns of supervision. In addition to such typologies, various accident scenarios have been defined in accident databases, such as the German In-Depth Accident Study (GIDAS).

In the STRADA database, the pedestrian trajectory, the car trajectory, and the location of the accident are the basic traffic elements used to define the car-pedestrian accident scenarios. Among these three traffic elements, the accident location (i.e., roadway or intersection) is the primary factor, the pedestrian trajectory is the secondary factor, and the car trajectory is comparatively less important. This classification has certain drawbacks. Primarily, some accidents in which the cars involved have notably different moving trajectories are classified under the same accident scenario. This problem precludes any discrimination of the car trajectories in the accident scenarios defined by the pedestrian trajectory (as in F3 and F4 in Table 4-1).

For evaluation of the remote pedestrian sensor system, an accident classification based on the pedestrian trajectory, the car trajectory, and the pedestrian visibility would be more useful. In this classification, the detailed pedestrian and car trajectories should be used equally as the major traffic elements for categorizing car-pedestrian accidents. The pedestrian visibility can be used as a secondary factor in this classification. Based on this accident classification, the performance of the remote sensor system can be assessed better.

5.3 Evaluation of Remote Sensor Performance

Considering the high cost and time consumption of field testing, statistical simulation methods were developed to assess remote pedestrian sensor systems. Wakim et al. (2004) presented a Monte-Carlo simulation tool to evaluate the performance of remote pedestrian sensor systems. Their study collected and classified vehicle-pedestrian crashes into 11 typical scenarios. The statistical behaviors of the key factors involved (i.e., vehicles, pedestrians, the environment, and the remote pedestrian sensor systems) were modeled respectively. The Monte-Carlo simulations were then conducted to calculate the probability of vehicle-pedestrian impacts being detected by the sensor systems.

In Paper I, a statistical simulation method was also developed to evaluate the remote pedestrian sensor system. However, the major difference between these two studies is the role played by the analysis of accident scenarios. In the study presented by Wakim et al. (2004), the analysis of accident scenarios is only a method to obtain the statistical behaviors of the important accident factors. In Paper I, the analysis of the accident scenarios not only serves as the basis for the development of knowledge about accidents, but also as the foundation for the statistical simulation. Based on the carefully selected accident scenarios, the complexity of the statistical models of the key accident factors can obviously be reduced and the reliability and feasibility of the statistical simulation can be improved. The statistical methods used in both studies do nothing to evaluate the robustness and accuracy of remote sensor systems. In the study of Wakim et al. (2004), the false alarm and correct detection rates were appointed directly and included in the simulation model as random variables. Paper I, on the other hand, assumed that no pedestrian in the detecting range of the sensor system would be missed or misinterpreted.

Cathey et al. (2007) described a method to evaluate comprehensively the performance of a pedestrian remote sensor system by using driving simulation technology. In their study, the driving simulation technology was used to create a virtual traffic environment. In this virtual environment, the characteristics and behaviors of pedestrians were presented. The output of the remote sensors in this traffic environment was then mimicked and post-processed to facilitate identification of pedestrians at risk. Using this method, the robustness and accuracy of the pedestrian remote sensor system could be evaluated comprehensively. In order to evaluate the performance of pedestrian remote sensor systems by this method, two studies should be extended further. The first should include an in-depth analysis of the pedestrian traffic environment and traffic behavior, which would allow for the traffic environment to be modeled reliably. The second study should include a field test of different pedestrian remote sensors in order to mimic sensor output accurately.

5.4 Pedestrian Contact Sensor

Mlekusch et al. (2004) presented a pressure sensor concept for the detection of pedestrian impacts. According to their concept, a small tube was fixed on the inner surface of the bumper cover. Both ends of

the tube were sealed by a pressure sensor, and the medium contained inside the tube was air. When the bumper was impacted by an object, the sensor tube was compressed and the impact signal was detected by the pressure sensors.

Paper II evaluated a similar sensor concept for the detection of pedestrian impacts. The only difference is that in Paper II, the sensor tube was built into the bumper foam. The benefit of implementing this kind of contact sensor is that the temperature-dependent change in bumper foam stiffness is compensated by the opposite change in the stiffness of the sensor tube, thus enabling the output signal of the new sensor to remain relatively stable. The major shortcoming of this contact sensor is its comparatively long reaction time to pedestrian impacts. Because the air is used as the medium in the sensor tube, the pressure signal can only travel in the sensor tube at a speed of 343 m/s. As a result, detection of pedestrian impacts will be delayed depending on the distance between the impact point and the pressure sensor. One solution to this problem could be achieved by distributing several pressure sensors evenly along the sensor tube, thereby reducing the distance between the possible impact point and the closest pressure sensor, thus decreasing signal delay.

5.5 Statistics for Experiment Design

Paper III investigated the efficiency of the RBS of different design configurations at various impact conditions for the protection of pedestrians' lower limbs. The statistical method of factorial experiment design (Box et al., 2005) was used to design the parameter study and investigate the effects of the design parameters. According to this method, the main effect of a parameter was calculated as the change in the average simulation result as the parameter varied from low to high levels. Subsequently, the hypothesis testing method was used to evaluate the statistical significance of the main effect. Using this method, the influences on the effectiveness of the RBS by the design parameters and impact conditions were calculated and the most important parameters were identified.

This method includes certain limitations. The first problem is that the variations of the design parameters are always limited. Otherwise, a large number of simulations must be conducted. The second problem is that the significance of a parameter depends on the range of its variation. Therefore, it is difficult to evaluate the relative importance of the different design parameters, especially for the parameters of different physical meanings. The third problem evident in this method is that the statistical relationship between the simulation responses and the design parameters cannot be established and the optimized values of the design parameters cannot be determined.

Paper IV used the response surface method (Box et al., 2005) to optimize the protective performance of the RH. In the variation ranges of selected design parameters, a parameter study was conducted to investigate the simulation results for different combinations of the design parameters. A response surface was then presented to correlate the results and the design parameters, and the unknown coefficients in the response surface were solved by the least squares method. In order to evaluate the accuracy of the response surface, simulations were conducted for several extra combinations of the design parameters. The simulation results were compared with the results predicted by the response surface to evaluate the accuracy of the response surface. Based on the developed response surface, the optimized values of the design parameters can be solved in the variation ranges of the parameters.

The advantages of the implementation of the response surface method are obvious. In the selected variation ranges of the design parameters, the relationship between the simulation results and the design parameters can be established based on the limited number of simulations; the optimized values of the design parameters in the variation ranges can be solved based on the response surface. However, a certain limitation remains in the response surface method in that it only establishes the relationship between the simulation results and the design parameters in the limited variation ranges of the design parameters. If the values of the design parameters are selected outside those ranges, the developed response surface model will no longer be valid, and a new response surface must be developed.

5.6 Implementation of Human Body Models

In Papers II and III, the human lower limb model was used in parallel with the EEVC lower legform model to evaluate the protective performance of the bumper models. In Paper II, the baseline production bumper model and the improved bumper model were evaluated initially using the legform model. The

results indicated that the improved bumper can meet EEVC acceptance requirements. After this analysis, the baseline and improved bumper models were further evaluated using the lower limb model. As the simulations proved, the improved bumper protects the pedestrian's knee joint much more efficiently. However, the improved design also induced an increased risk of damage to the pedestrian's tibia. Paper III identified that under the same impact conditions, the peak tibia accelerations of the standard EEVC legform model and the human lower limb model were comparable. However, the peak knee-bending angle of the lower limb model was more than twice that of the legform model. The peak knee-shearing displacement of the lower limb model was two to eight times that of the legform model. The bio-fidelity of the EEVC lower legform impactor is poor for knee kinematics.

Paper IV used the adult human head model in parallel with the EEVC adult headform model to evaluate the safety performance of the RH. It identified that under the same impact conditions, the HIC value of the human head model coincided with that of the headform model. The change in the intracranial pressure of the human head model can predict the change in the HIC values of the human head model and the headform model.

The EEVC pedestrian subsystem impactors are EuroNCAP-required test instruments in evaluating the performance of pedestrian protection afforded by the car front. Thus, the FE models of the adult headform and lower legform impactors were used as the primary tools to evaluate and optimize the protective performance of the bumpers and the hood. Furthermore, the FE models of the human head and lower limb were also used to evaluate the bumpers and hood. Compared with the impactor models, the human body models represent the actual human body structures with higher bio-fidelity. The impact responses of the human body models indicate not only the severity of the injuries but also the detailed locations and mechanisms of the injuries. Therefore, human body models represent the development of future injury assessment tools.

5.7 Protective Performance of the RBS and RH

In order to alleviate the pedestrian injuries caused by collisions with the car bumper, a new bumper system was presented that would absorb the impact energy more efficiently. The basic design of the energy absorption bumper was based on an energy absorber made of foam or plastics, and was located between the stiff bumper beam and the bumper cover to absorb impact energy (Shuler and Staines, 1998; Kalliske and Friesen, 2001; Chon et al., 2007; Doerr et al., 2007; Jaarda and Nagwanshi, 2007; Pinecki and Zeitouni, 2007; Glance and Tokarz, 2008; Davies et al., 2009). The lower stiffener was also strengthened and moved forward to dissipate some of the impact energy (Shuler and Staines, 1998; Chon et al., 2007; Doerr et al., 2007; Pinecki and Zeitouni, 2007).

Paper III developed an RBS model from the original car bumper model. In this model, the connection between the bumper beam and the car frontal longitudinal beams was defined as the combination of translational joints and motors. The translational joints constrained the relative motion between the RBS and the car body in the longitudinal direction of the car body. The translational motors actuated the RBS extending to the desired place and at the desired speed. In order to improve the efficiency of the RBS to absorb impact energy, the thickness of the bumper foam was increased. To reduce the knee-bending angle, the lower stiffener was moved forward and connected with the bumper beam using five steel plates. The material used in the improved lower stiffener was also changed to steel. The EEVC lower legform model and the human lower extremity model were then used to study the influence of the stiffness, deploying speed, and deployed distance on the protective performance of the RBS. It was determined ultimately that the performance of the RBS can be improved by reducing bumper stiffness; however, the bumper performance is impaired during the deploying process. The deployment distance has no direct influence on the protective performance of the RBS.

In order to protect the pedestrian's head from collisions with the car hood, the active hood was implemented to soften the collision (Fredriksson et al., 2001; Kalliske and Friesen, 2001; Krenn et al., 2003; Lee et al., 2007; Pinecki and Zeitouni, 2007; Oh et al., 2008; Shin et al., 2008; Inomata et al., 2009). This system consists of a hood that lifts at the rear when a pedestrian is struck by the car. In this case, the distance between the hood and the stiff inner parts of the car (e.g. the engine) becomes wider, creating a larger degree of hood deformation when the hood is struck by the pedestrian's head and chest. As a result, more impact energy can be absorbed and pedestrian injuries can be alleviated.

Based on the active hood, the RH was further presented in Paper IV. When the risk of a pedestrian collision is detected by a remote pedestrian sensor system, the rear end of the RH is lifted to protect the pedestrian's head, similar as the active hood. If the collision is avoided, the lifted rear end of the RH can be retracted to protect against future accidents. Paper IV used the response surface method to optimize the protective performance of the RH. The EEVC headform and the human head models were used to evaluate the protective performance of RH. The study determined that compared to the retracted baseline RH, the lifted baseline RH can reduce the impact responses of the headform and human head models. However, the lifting baseline RH can increase the impact responses of the headform and human head models. Given the reduced lifting speed and increased lifted height, the optimized RH can meet the acceptance requirement of EEVC WG17 of HIC values lower than 1,000.

According to the literature review, the same protective performance for pedestrians' lower limbs and heads can be achieved using the energy absorption bumper and the active hood. However, other benefits can be obtained through implementation of the RBS and RH as well. For example, the RBS can also be deployed in frontal car crashes to absorb part of the impact energy, which would otherwise be transferred to car occupants. Furthermore, the RBS and RH can be reused to deploy in lower risk situations and before pedestrian collisions.

5.8 Recommendation of Future Studies

Using statistical simulation method, Paper I evaluated the effectiveness of the remote sensor system for detecting pedestrians at risk in specific vehicle traffic environment. As discussed in section 5.1, the accident data missed in the STRADA database can lead to the error of sensor evaluation. In order to evaluate the remote pedestrian sensor system more accurately, the accident factors listed in Table 5-1 should be investigated. As indicated by this table, most factors have been recorded completely or partially recorded in the STRADA database; however, many important factors are still missing. This missing information should be investigated in future studies. As discussed in section 5.3, the statistical simulation method used in Paper I do nothing to evaluate the robustness and accuracy of the remote sensor system. For this reason, a field test should be conducted in the future to investigate the sensor effectiveness in real traffic environment. Otherwise, a simulation study presented by Cathey et al. (2007) can be used to evaluate the sensor effectiveness.

Table 5-1 Accident factors important for the evaluation of the remote sensor system

Factor		STRADA Record
Pedestrian	Age	Yes
	Size (weight/stature)	No
	Clothes	No
	Trajectory	Yes
	Gait	No
	Visibility	No
	Thrown distance	No
	Injury type	Partly
	Injury severity	Partly
Vehicle	Type	Yes
	Trajectory	Yes
	Velocity	No
	Braking	No
	Damage	No
Environment	Weather	Yes
	Light condition	Yes
	Road surface	Yes
	Road slope	No
	Road curvature	No
	Road speed limit	Yes
	Skid mark	No
	Accident scene (urban/country)	Yes
	Accident location (roadway/intersection)	Yes

In Paper III, the human lower limb model was used in parallel with the EEVC lower legform model to investigate the efficiency of the RBS of different design configurations in various impact conditions. In Paper IV, the human head model and the EEVC adult headform model were used to evaluate and optimize

the RH for the prevention of the head injuries of an adult pedestrian from hood collisions at certain impact points. However, the collisions between the overall pedestrian body and the adaptive car front were not studied. The probable risk of severe pedestrian injuries, such as the severe head injuries from the collisions between the pedestrian head and the rear edge of the RH, were therefore not investigated. In the future study, the collisions between the overall pedestrian body and the RH should be analyzed to confirm the safety benefit of the adaptive car front.

6. CONCLUSIONS

This study contributed to the evaluation and optimization of the performance of an integrated pedestrian safety system. A remote sensor system and a contact sensor were evaluated for the detection of pedestrian impacts. An RBS and an RH were then evaluated and optimized relative to the protection of pedestrians during car collisions. The major conclusions in this study are summarized as follows:

- The two most common scenarios for pedestrian accidents in Sweden are cars entering and leaving intersections and colliding with pedestrians crossing the road, accounting for 46.8% of the 2,199 selected cases.
- The remote sensor system can detect almost all visible pedestrians in these two most common scenarios in a timely manner as long as the detection angle is greater than 60 degrees.
- The baseline bumper model failed to meet the acceptance requirements of the EEVC WG17 lower legform tests. By improving the bumper design, the protective performance of the bumper model was enhanced, and the results of virtual testing met EEVC requirements. After further evaluation using the human lower limb model, the improved bumper model was found to protect pedestrians' lower limbs better than the baseline bumper model.
- Built into the improved bumper model, the contact sensor can identify pedestrian impacts to the car bumper. Moreover, the enhanced sensor output stability and mass sensitivity can be achieved by using a 25 mm rather than a 50 mm sensor tube.
- The performance of the RBS for the protection of pedestrians' lower limbs can be improved by reducing bumper stiffness. The protective performance of the RBS is impaired during the deployment process by a speed of 2.5 m/s or greater. Less than 150 mm, the maximum deployment distance of the specific RBS has no influence on the bumper performance.
- Compared with the retracted and lifting baseline RH, the lifted baseline hood can definitely minimize the injury parameters from the headform and human head models. This indicates a potential for the reduction in the risk of pedestrian fatality from head impacts.
- The further reduction of the impact responses of the headform and human head models can be obtained by using the optimized rather than the baseline RH. When the optimized RH is lifted, the HIC values of the headform and human head models are reduced to levels much lower than 1,000. Therefore, the risk of pedestrian head injuries can be prevented as required by EEVC WG17.

REFERENCES

Advani S.H., Ommaya A.K. and Yang W.J. (1982) Head injury mechanisms, characteristics and clinical evaluation, Human Body Dynamics Oxford Medical Engineering Series, Clarendon, Oxford

Allsop D.L., Perl D.R. and Warner C.Y. (1991) Force/Deflection and Fracture Characteristics of the Tomporo-Parietal Region of the Human Head, 35th Stapp Car Crash Conf., San Diego, USA

Al-Ghamdi A.S. (2002) Pedestrian-Vehicle Crashes and Analytical Techniques for Stratified Contingency Tables, Accident Analysis and Prevention, Vol. 34, No. 2, pp. 205-214

Anderson R.W.G., Mclean A.J., Farmer M.J.B., Lee B.H. and Brooks C.G. (1997) Vehicle Travel Speeds and the Incidence of Fatal Pedestrian Crashes, Accident Analysis and Prevention, Vol. 29, No. 5, pp. 667-674

Ashton S.J. (1980) A Preliminary Assessment of the Potential for Pedestrian Injury Reduction through Vehicle Design, 24th Stapp Car Crash Conf., Troy, USA

Assailly J.P. (1997) Characterization and Prevention of Child Pedestrian Accidents: An Overview, Journal of Applied Developmental Psychology, Vol. 18, No. 2, pp. 257-262

Barton B.K. and Schwebel D.C. (2007) The Roles of Age, Gender, Inhibitory Control, and Parental Supervision in Children's Pedestrian Safety, Journal of Pediatric Psychology, Vol. 32, No.5, pp. 517–526

Beillas P., Begeman P.C., Yang K.H., King A.I., Arnoux P.J., Kang H.S., Kayvantash K., Brunet C., Cavallero C. and Prasad P. (2001) Lower Limb: Advanced FE Model and New Experimental Data, 45th Stapp Car Crash Conf., San Antonio, USA

Bertozzi M., Broggi A., Chapuis R., Chausse F., Fascioli A. and Tibaldi A. (2003) Shape-Based Pedestrian Detection and Localization, Proc. of IEEE Intelligent Transportation Systems, Vol. 1, pp. 328- 333

Bovenkerk J., Sahr C., Zander O. and Kalliske I. (2009) New Modular Assessment Methods for Pedestrian Protection in the Event of Head Impacts in the Windscreen Area, 21st Int. Technical Conf. on the Enhanced Safety of Vehicles, Stuttgart, Germany

Box E.G., Hunter S.J. and Hunter G.W. (2005) Statistics for Experimenters Design, Innovation, and Discoevery, 2nd Edition, New York: John Wiley & Sons

Bu F. and Chan C. (2005) Pedestrian Detection in Transit Bus Application: Sensing Technologies and Safety Solutions, Proc. of IEEE Intelligent Vehicles Symposium, pp. 100-105

Bunketorp O., Aldman B., Thorngren L. and Romansu B. (1982) Clinical and Experimental Studies of Leg Injuries in Car-Pedestrian Accidents, 9th Int. Technical Conf. on Experimental Safety Vehicle, Kyoto, Japan

Cathey L., Steiger R., Wallis C., Lopez M. and Blommer M. (2007) Real Time Simulation of Virtual Pedestrians for Development of Pedestrian Detection Systems, SAE World Congress, Detroit, USA

Chen H.P., Fu L.X. and Zheng H.Y. (2009) A Comparative Study between China and IHRA for the Vehicle-Pedestrian Impact, SAE World Congress, Detroit, USA

Chen Y.X. and Han C.Z. (2008) Night-time Pedestrian Detection by Visual-Infrared Video Fusion, Proc. of the 7th World Congress on Intelligent Control and Automation, Chongqing, China

Chon D., Uikey D. and Mohammed R.A. (2007) Energy Absorber Developments and Correlation for Lower Leg Pedestrian Impact, SAE World Congress, Detroit, USA

Cuerden R., Richards D., Hill J. (2007) Pedestrians and Their Survivability at Different Impact Speeds, 20th Int. Technical Conf. on Enhanced Safety Vehicle, Lyon, France

Cutler R. and Davis L. (1999) Real-Time Periodic Motion Detection, Analysis and Applications, Proc. of IEEE Conf. on Computer and Pattern Recognition, pp. 326-331

Davies H., Holford K., Assoune A., Trioulier B. and Courtney B. (2009) Pedestrian Protection Using A Shock Absorbing Liquid (SALi) Based Bumper System, 21st Int. Technical Conf. on the Enhanced Safety of Vehicles, Stuttgart, Germany

Davis G. A. (2001) Relating Severity of Pedestrian Injury to Impact Speed in Vehicle-Pedestrian Crashes: Simple Threshold Model, Transportation Research Record, n 1773, pp. 108-113

Deck C., Nicolle S. and Willinger R. (2004) Human Head FE Modeling: Improvement of Skull Geometry and Brain Constitutive Laws, Proc. of Int. IRCOBI Conf. Biomechanics of Impact, pp. 79-92

Doerr R., Huda N., Newlands G. and Keer T. (2007) Development of Expanded Polypropylene (EPP) Bumper Systems to Meet Emerging Performance and Safety Standards, SAE World Congress, Detroit, USA

Edwards K. J. and Green J. F. (1999) Analysis of the Inter-relationship of Pedestrian Leg and Pelvis Injuries, Proc. of Int. IRCOBI Conf. Biomechanics of Impact, pp. 355-369

EEVC (2002) Improved Test Methods to Evaluate Pedestrian Protection Affordable by Passenger Cars, European Enhanced Vehicle-safety Committee, Working Group 17 Report, Dec. 1998 with Sep.2002 updates

Ejima S., Nishimoto T., Yuge K., Tomonaga K., Murakami S. and Takao H. (2004) Three-Dimensional Human-Head Model using VOXEL Approach Developed for Head-Injury Analysis, Digital Human Modeling Symposium, Oakland, USA

Eppinger R., Sun E., Kuppa S. and Saul R.: Supplement (2000) Development of Improved Injury Criteria for the Assessment of Advanced Automotive Restraint Systems-II, National Highway Traffic Safety Administration, Department of Transportation, Washington DC, USA

ERSO (2008) Traffic Safety Basic Facts 2008 – Pedestrians, European Road Safety Observatory, http://www.erso.eu/safetynet/fixed/WP1/2008/BFS2008_SN-KfV-1-3-Pedestrians.pdf, Accessed 2009-09-10

European Parliament and Council (2009) Regulation (EC) No 78/2009 of the European Parliament and of the Council, Official Journal of the European Union

Fardi B., Schuenert U. and Wanielik G. (2005) Shape and Motion-Based Pedestrian Detection in Infrared Images: A Multi Sensor Approach, Proc. of IEEE Intelligent Vehicles Symposium, pp. 18-23

Fontaine H. and Gourlet Y. (1997) Fatal Pedestrian Accidents in France: A Typological Analysis, Accident Analysis and Prevention, Vol. 29, No. 3, pp. 303-312

Foret-Bruno J-Y, Faverjon G. and Coz L. J-Y (1998) Injury Pattern of Pedestrians Hit by Cars of Recent Design, Proc. of the 16th Int. Technical Conf. on the Enhanced Safety of Vehicles, pp. 2122-2130, Windsor, Canada

Fredriksson R., Håland I. and Yang J. K. (2001) Evaluation of a New Pedestrian Head Injury Protection System with a Sensor in the Bumper and Lifting of the Bonnet's Rear Edges, 17th Int. Technical Conf. on the Enhanced Safety of Vehicles, Amsterdam, the Netherlands

Gandhi T. and Trivedi M.M. (2006) Pedestrian Collision Avoidance Systems: A Survey of Computer Vision Based Recent Studies, Proc. of IEEE Intelligent Transportation Systems Conf. (ITSC), pp. 976-981

Gavrila D.M. and Giebel J. (2002) Shape-Based Pedestrian Detection and Tracking, Proc. of IEEE Intelligent Vehicles Symposium, Vol. 1, pp. 8-14

Gavrila D.M., Kunert M. and Lages U. (2001) A Multi-sensor Approach for the Protection of Vulnerable Traffic Participants the PROTECTOR Project, Proc. of the 18th IEEE Instrumentation and Measurement Technology Conf., Vol. 3, pp. 2044-2048

Gidel S., Blanc C., Chateau T., Checchin P. and Trassoudaine L. (2009) Non-parametric Laser and Video Data Fusion: Application to Pedestrian Detection in Urban Environment, 12th Int. Conf. on Information Fusion, Seattle, USA

Glance P. and Tokarz B. (2008) Evaluation of a New Tubular Energy Absorber Designed to Meet Bumper System Pedestrian Lower Leg Impact and 5 & 6 MPH Impact Series Requirements, SAE World Congress, Detroit, USA

Gorrie C.A., Brown J. and Waite P.M.E. (2008) Crash Characteristics of Older Pedestrian Fatalities: Dementia Pathology May Be Related to 'at Risk' Traffic Situations, Accident Analysis and Prevention, Vol. 40, No. 3, pp. 912-919

Guo R., Yuan Q., Sturgess C.E.N., Hassan A.M., Li Y. and Hu Y. (2006) A Study of an Asian Anthropometric Pedestrian in Vehicle-Pedestrian Accidents Using Real-World Accident Data, International Journal of Crashworthiness, Vol. 11, No. 6, pp. 541-551

Gurdjian E., Lissner H., Latimer R., Haddad B. and Webster J. (1953) Quantitative Determination of Acceleration and Intracranial Pressure in Experimental Head Injury, Neurology, Vol. 3(6), pp. 417-423

Gurdjian E., Robert V., Thomas L. (1966) Tolerance Curves of Acceleration and Intracranial Pressure and Protective Index in Experimental Head Injury, Journal of Trauma, Vol. 6(5), pp. 600-604

Gårder P.E. (2004) The Impact of Speed and Other Variables on Pedestrian Safety in Maine, Accident Analysis and Prevention, Vol. 36, No. 4, pp. 533-542

Harruff C. R., Avery A. and Alter-Pandya S. A. (1998) Analysis of Circumstances and Injuries in 217 Pedestrian Traffic Fatalities, Accident Analysis and Prevention, Vol. 30, No.1, pp. 11-20

Hodgson V.R. and Thomas L.M. (1971) Comparison of Head Acceleration Injury Indices in Cadaver Skull Fracture, 15th Stapp Car Crash Conf., San Diego, USA

Holding P.N., Chinn B.P. and Happian-Smith J. (2001) Pedestrian Protection - An Evaluation of an Airbag System through Modeling and Testing, 17th Int. Technical Conf. on the Enhanced Safety of Vehicles, Amsterdam, the Netherlands

Holland C. and Hill R. (2010) Gender Differences in Factors Predicting Unsafe Crossing Decisions in Adult Pedestrians across the Lifespan: A Simulation Study, Accident Analysis and Prevention, doi: 10.1016/j.aap.2009.12.023

Holubowycz O.T. (1995) Age, Sex, and Blood Alcohol Concentration of Killed and Injured Pedestrians, Accident Analysis and Prevention, Vol. 27, No.3, pp. 417-422

Huang Y., King A.I. and Cavanaugh J.M. (1994) Finite Element Modeling of Gross Motion of Human Cadavers in Side Impact, 38th STAPP Car Conf., Ft. Lauderdale, USA

Huang S.N., Yang J.K. and Fredriksson R. (2008): Performance Analysis of a Bumper-Pedestrian Contact Sensor System by Using FE Models, Int. Journal of Crashworthiness, Vol. 13, No. 2, pp. 149-157

Inomata Y., Iwai N., Maeda Y., Kobayashi S., Okuyama H. and Takahashi N. (2009) Development of the Pop-Up Hood for Pedestrian Head Protection, 21st Int. Technical Conf. on the Enhanced Safety of Vehicles, Stuttgart, Germany

ITARDA (2004) Pedestrian Traffic Accidents, Institute for Traffic Accident Research and Data Analysis in Japan, http://www.itarda.or.jp/english/info50/50top.html, Accessed 2009-09-10

Ivarsson B.J., Genovese D., Crandall J.R., Bolton J.R., Untaroiu C.D. and Bose D. (2009) The Tolerance of the Femoral Shaft in Combined Axial Compression and Bending Loading, Stapp Car Crash Journal, Vol. 53, pp. 251-290

Iwamoto M., Kisanuki Y., Watanabe I., Furusu K., Miki K. and Hasegawa J. (2002) Development of a Finite Element Model of the Total Human Model for Safety (THUMS) and Application to Injury Reconstruction, 2002 Int. IRCOBI Conf. on the Biomechanics of Impact, Munich, Germany

Iwamoto M., Tamura A., Furusu K., Kato C., Miki K., Hasegawa J. and Yang K.H. (2000) Development of a Finite Element Model of the Human Lower Limb for Analyses of Automotive Crash Injuries, SAE World Congress, Detroit, USA

Jaarda E. and Nagwanshi D. (2007) Prototype Design and Testing of a Global Energy Absorber Concept for Coupled Pedestrian and Vehicle Protection, SAE World Congress, Detroit, USA

Kajzer J., Cavallero C., Bonnoit J., Morjane A. and Ghanouchi S. (1993) Response of the Knee Joint in Lateral Impact: Effect of Bending Moment, Proc. Int. IRCOBI Conf. Biomechanics of Impact, pp. 105-116

Kajzer J., Cavallero C., Ghanouchi S., Bonnoit J. and Ghorbel A. (1990) Response of the Knee Joint in Lateral Impact: Effect of Shearing Loads, Proc. Int. IRCOBI Conf. Biomechanics of Impact, pp. 293-304

Kajzer J., Matsui Y., Ishikawa H., Schroeder G. and Bosch U. (1999) Shearing and Bending Effects at the Knee Joint at Low-speed Lateral Loading, Occupant Protection SP 1432, pp. 1-12

Kajzer J., Schroeder G., Ishikawa H. Matsui Y. and Bosch U. (1997) Shearing and Bending Effects at the Knee Joint at High-speed Lateral Loading, 41st Stapp Car Crash Conf., Lake Buena Vista, USA

Kalliske I. and Friesen F. (2001) Improvements to Pedestrian Protection as Exemplified on a Standard-Sized Car, 17th Int. Technical Conf. on the Enhanced Safety of Vehicles, Amsterdam, the Netherlands

Kang H.S., Willinger R., Diaw B.M. and Chinn B. (1997) Validation of a 3D Anatomic Human Head Model and Replication of Head Impact in Motorcycle Accident by Finite Element Modeling, 41st Stapp Car Crash Conf., Lake Buena Vista, USA

Kikuchi Y., Takahashi Y. and Mori F. (2006) Development of a Finite Element Model for a Pedestrian Pelvis and Lower Limb, SAE World Congress, Detroit, USA

Kim A.C. and Chang F. (2005) Rapid Detection and Identification of Pedestrian Impacts Using a Distributed Sensor Network, Proc. of SPIE, Vol. 5764, Smart Structures and Materials 2005: Smart Structures and Integrated Systems, pp. 80-91

Kimpara H., Lee J.B., Yang K.H., King A.I., Iwamoto M., Watanabe I. and Miki K. (2005) Development of a Three-Dimensional Finite Element Chest Model for the 5th Female, 49th STAPP Car Crash Conf., Washington DC, USA

Kleiven S. and Hardy W.N. (2002) Correlation of an FE Model of the Human Head with Local Brain Motion-Consequences for Injury Prediction, 46th Stapp Car Crash Conf., Ponte Verdra Beach, USA

Knoblauch R.L. and Knoblauch B.D. (1976) Urban Pedestrian Accident Data Base, Final Report to the National Highway Traffic Safety Administration, DOT HS-190-2-480, Washington DC, USA

Kong C.Y. and Yang J.K. (2010) Logistic Regression Analysis of Pedestrian Casualty Risk in Passenger Vehicle Collisions in China, Accident Analysis and Prevention, doi: 10.1016/j.aap.2009.11.006

Kramlich T., Langwieder K., lang D., and Hell W. (2002) Accident Characteristics in Car-to-Pedestrian Impacts, 2002 Int. IRCOBI Conf. on the Biomechanics of Impact, Munich, Germany

Krammer M., Burow K. and Heger A. (1973) Fracture Mechanisms of Lower Legs under Impact Load, 17th Stapp Car Crash Conf., Oklahoma City, USA

Krenn M., Mlekusch B., Wilfling K., Dobida F. and Deutscher E. (2003) Development and Evaluation of a Kinematic Hood for Pedestrian Protection, SAE World Congress, Detroit, USA

Kress T.A. and Porta D.J. (2001) Characterization of Leg Injuries from Motor Vehicle Impacts, 17th Int. Technical Conf. on Enhanced Safety Vehicle, Amsterdam, the Netherlands

Kress T.A., Porta D.J., Snider J.N., Fuller P.M., Psihogios J.P., Heck W.L., Frick S.J. and Wasserman J.F. (1995) Fracture Patterns of Human Cadaver Long Bones, Int. IRCOBI Conf. Biomechanics of Impact, Brunnen, Switzerland

Kress T.A., Snider J.N., Porta D.J., Fuller P.M., Wasserman J.F. and Tucker G.V. (1993) Human Femur Response to Impact Loading, Proc. Int. IRCOBI Conf. Biomechanics of Impact, pp. 93-104

Krotosky S.J. and Trivedi M.M. (2007) A Comparison of Color and Infrared Stereo Approaches to Pedestrian Detection, Proc. of the 2007 IEEE Intelligent Vehicles Symposium, pp. 81-86

Labayrade R., Royere C., Gruyer D. and Aubert D. (2005) Cooperative Fusion for Multi-Obstacles Detection with Use of Stereovision and Laser Scanner, Autonomous Robots, Vol. 19, No. 2, pp. 117-140

Lee K.B., Jung H.J. and Bae H. (2007) The Study on Developing Active Hood Lift System for Decreasing Pedestrian Head Injury, 20th Int. Technical Conf. on Enhanced Safety Vehicle, Lyon, France

Li F. and Yang J.K. (2007) Parameter Study on Head Protection in Vehicle-Pedestrian Collision, China Mechanical Engineering, Vol. 18, No. 9, pp. 1125-1130

Linzmeier D.T., Skutek M., Mekhaiel M. and Dietmayer K.C.J. (2005) A Pedestrian Detection System based on Thermopile and Radar Sensor Data Fusion, 7th Int. Conf. on Information Fusion, Philadelphia, USA

Lissner H., Lebow M. and Evans F. (1960) Experimental Studies on the Relation between Acceleration and Intracranial Pressure Changes in Man, Surg Gynecol Obstet, Vol. 111, pp. 320-338

Lizee E., Robin S., Song E., Bertholon N., Coz J.-Y. L., Besnault B. and Lavaste F. (1998) Development of a 3D Finite Element Model of the Human Body, 42nd STAPP Car Crash Conf., Tempe, USA

Lobjois R. and Cavallo V. (2009) The Effects of Aging on Street-Crossing Behavior: From Estimation to Actual Crossing, Accident Analysis and Prevention, Vol. 41, No. 2, pp. 259-267

Longhitano D., Henary B., Bhalla K., Ivarsson J. and Crandall J. (2005) Influence of Vehicle Body Type on Pedestrian Injury Distribution, SAE World Congress, Detroit, USA

Löwenhielm P. (1974) Strain Tolerance of the Vv. Cerebri Sup (Bridging Veins) Calculated from Head-on Collision Tests with Cadavers, Z. Rechtsmedizin, Vol. 75, No. 2, pp. 131-141

LSTC (2006) LS_DYNA Theory Manual, http://www.lstc.com/manuals.htm, Accessed 2010-02-10

LSTC (2007) LS_DYNA Keyword User's Manual, http://www.lstc.com/manuals.htm, Accessed 2010-02-10

Maeno T. and Hasegawa J. (2001) Development of a Finite Element Model of the Total Human Model for Safety (THUMS) and Application to Car-Pedestrian Impacts, 17th Int. Technical Conf. on the Enhanced Safety of Vehicles, Amsterdam, the Netherlands

Maki T. and Asai T. (2002) Development of Pedestrian Protection Technologies for ASV, JASE Review, Vol. 23, No. 3, pp. 353-356

Maki T., Kajzer J., Mizuno K. and Sekine Y. (2003) Comparative Analysis of Vehicle-Bicyclist and Vehicle-Pedestrian Accidents in Japan, Accident Analysis and Prevention, Vol. 35, No. 6, pp. 927-940

McCarthy M. and Simmons I. (2005) Active Pedestrian Protection, 19th Int. Technical Conf. on the Enhanced Safety of Vehicles, Washington DC, USA

Mertz H.J., Prasad P. and Nusholtz G. (1996) Head Injury Risk Assessment for Forehead Impacts, SAE Int. Congress and Exposition, Detroit, USA

Mizuno K. and Kajzer J. (2000) Head Injuries in Vehicle-Pedestrian Impact, SAE Transactions 2000, Vol. 109, No. 6, pp. 232-243

Mizuno K., Yonezawa H. and Kajzer J. (2001) Pedestrian Headform Impact Tests for Various Vehicle Locations, 17th Int. Technical Conf. on the Enhanced Safety of Vehicles, Amsterdam, the Netherlands

Mizuno Y. (2005) Summary of IHRA Pedestrian Safety WG Activities (2005) – Proposed Test Methods to Evaluate Pedestrian Protection Afforded by Passenger Cars, 19th Int. Technical Conf. on the Enhanced Safety of Vehicles, Washington DC, USA

Mlekusch B., Wilfling C., Gröger U., Dukart A. and Mack F. (2004) Active Pedestrian Protection – System Development, 2004 SAE World Congress, Detroit, USA

Mori H., Charkari N. M. and Matsushita T. (1994) On Line Vehicle and Pedestrian Detection Based on Sign Pattern, IEEE Transaction on Industrial Electronics, Vol. 41, No. 4, pp. 384-391

Moxey E., Johnson N., McCarthy M. G., Galloway L., Parker G. A. and McLundie W. M. (2006) Advanced Protection for Vulnerable Road Users: A Case Study, Proc. of the I MECH E Part D Journal of Automobile Engineering, Volume 220(6), pp. 723-734(12)

Nagasaka K., Mizuno K., Tanaka E., Yamamoto S., Iwamoto M., Miki K. and Kajzer J. (2003) Finite Element Analysis of Knee Injury Risk in Car-to-Pedestrian Impacts, Traffic Injury Prevention, Vol. 4, No. 4, pp. 345-354

Nahum A.M., Gatts J.D., Gadd C.W. and Danforth J. (1968) Impact Tolerance of the Skull and Face, 12th Stapp Car Crash Conf., Detroit, USA

Nahum A.M. and Melvin J.W. (2001) Accident Injury: Biomechanics and Prevention, New York: Springer-Verlag

Nahun A.M., Smith R.W., Ward C.C. (1977) Intracranial Pressure Dynamics during Head Impact, 21st Stapp Car Crash Conf., New Orleans, Louisiana, USA

Natroshvili K., Schmid M., Stephan M., Stiegler A., and Schamm T. (2008) Real Time Pedestrian Detection by Fusing PMD and CMOS Cameras, 2008 IEEE Intelligent Vehicles Symposium, Eindhoven, the Netherlands

NHTSA (2008a) Traffic Safety Facts 2007 – Pedestrians, National Highway Traffic Safety Administration, National Highway Traffic Safety Administration, Department of Transportation, Washington DC, USA

NHTSA (2008b) Traffic Safety Facts 2007 – Overview, National Highway Traffic Safety Administration, National Highway Traffic Safety Administration, Department of Transportation, Washington DC, USA

NHTSA (2008c) Traffic Safety Facts 2007 – A Compilation of Motor Vehicle Crash Data from the Fatality Analysis Reporting System and the General Estimates System, National Highway Traffic Safety Administration, Department of Transportation Washington DC, USA

Niyogi S.A. and Adelson E.H. (1994) Analyzing and Recognizing Walking Figures in XYT, Proc. of IEEE Conf. on Computer Vision and Pattern Recognition, pp. 469-474

Nyquist G.W., Cavanaugh J.M., Goldberg S.J. and King A.I. (1986) Facial Impact Tolerance and Response, 30th Stapp Car Crash Conf., San Diego, USA

Nyquist G.W., Cheng R., EI-Bohy A.A.R. and King A.I. (1985) Tibia Bending: Strength and Response, 29th Stapp Car Crash Conf., Washington DC, USA

Oh C., Kang Y. and Kim W. (2008) Assessing the Safety Benefits of an Advanced Vehicular Technology for Protecting Pedestrians, Accident Analysis and Prevention, Vol. 40, No. 3, pp. 935-942

Ommaya A.K., Yarnell P., Hirsch A.E. and Harris E.H. (1967) Scaling of Experimental Data on Cerebral Concussion in Sub-Human Primates to Concussion Threshold for Man, 11th Stapp Car Crash Conf., Anaheim, USA

Oxley J., Fildes B., Ihsen E., Charlton J. and Day R. (1997) Differences in Traffic Judgments between Young and Old Adult Pedestrians, Accident Analysis and Prevention, Vol. 29, No. 6, pp. 839-847

Pinecki C. and Zeitouni R. (2007) Technical Solutions for Enhancing the Pedestrian Protection, 20th Int. Technical Conf. on the Enhanced Safety of Vehicles, Lyon, France

Ramanan D., Forsyth D. A. and Zisserman A. (2007) Tracking People by Learning Their Appearance, IEEE Transactions on Pattern Analysis and Machine Intelligence, Vol. 29, No. 1, pp. 65-81

Ramet M., Bouquet R., Bermond F., Caire Y. and Bouallegue M. (1995) Shearing and Bending Human Knee Joint Tests in Quasi-Static Lateral Load, Proc. Int. IRCOBI Conf. Biomechanics of Impact, pp. 93-105

Richards D., Cookson R., Cuerden R. and Davies G. (2009) The Causes of Pedestrians' Head Injuries following Collisions with Cars Registered in 2000 or later, 21st Int. Technical Conf. on the Enhanced Safety of Vehicles, Stuttgart, Germany

Robin S. (2001) HUMOS: Human Model for Safety–A Joint Effort towards the Development of Refined Human-Like Car Occupant Models, 17th Int. Technical Conf. on the Enhanced Safety of Vehicles, Amsterdam, the Netherlands

Rooij L., Hoof J.V., McCann M.J., Ridella S.A., Rupp J.D., Barbir A., Made R.V.D. and Slaats P. (2004) A Finite Element Lower Limb and Pelvis Model for Predicting Bone Injuries due to Knee Bolster Loading, Digital Human Modeling Symposium, Oakland, USA

Rosen E. and Sander U. (2009) Pedestrian Fatality Risk as a Function of Car Impact Speed, Accident Analysis and Prevention, Vol. 41, No. 3, pp. 536-542

Ruan J., EI-Jawahri R., Chai L., Barbat S. and Prasad P. (2003) Prediction and Analysis of Human Thoractic Impact Responses and Injuries in Cadaver Impacts Using a Full Human Body Finite Element Model, 47th Stapp Car Crash Conference, San Diego, USA

Ruan J.S., Khalil T.B. and King A.I. (1996) Impact Head Injury Analysis Using an Explicit Finite Element Human Head Model, Journal of Traffic Medicine, Vol. 25, No. 1/2, pp. 33-40

SAE (1980) Human Tolerance to Impact Conditions as Related to Motor Vehicle Design, SAE J885 APR80, Report, Warrendale, USA

Scherf O. (2005) Development and Performance of Contact Sensors for Active Pedestrian Protection Systems, 19th Int. Technical Conf. on the Enhanced Safety of Vehicles, Washington DC, USA

Schmitt K.-U., Niederer P. and Walz F. (2004) Trauma Biomechanics: Introduction to Accidental Injury, Berlin, Heidelberg and New York: Springer-Verlag

Schneider D.C. and Nahum A.M. (1972) Impact Studies of Facial Bones and Skull, 16th Stapp Car Crash Conf., Detroit, USA

Schofer L.J., Christoffel K.K., Donovan M., Lavigne V.J., Tanz R.R. and Wills E.K. (1995) Child Pedestrian Injury Taxonomy Based on Visibility and Action', Accident Analysis and Prevention, Vol. 27, No. 3, pp. 317-333

Schreiber P., Crandall J., Micek T., Hurwitz S. and Nusholtz G.S. (1997) Static and Dynamic Bending Stress of the Leg, Proc. Int. IRCOBI Conf. Biomechanics of Impact, pp. 99-113

Schuster P.J., Chou C.C., Prasad P. and Jayaraman G. (2000) Development and Validation of a Pedestrian Lower Limb Non-Linear 3-D Finite Element Model, 44th Stapp Car Crash Conf., Atlanta, USA

Shin M.K., Park K.T. and Park G.J. (2008) Design of Active Hood Lift System Using Orthogonal Arrays, Proc. of the Institution of Mechanical Engineers, Part D, Journal of automobile engineering, Vol. 222, No. 5, pp. 705-717

Shuler P.J. and Staines B. (1998) Determination of Bumper Styling and Engineering Parameters to Reduce Pedestrian Leg Injuries, SAE World Congress, Detroit, USA

Snyder M.B. and Knoblauch R.L. (1971) Pedestrian Safety: The Identification of Precipitating Factors and Possible Countermeasures (Vol.1), Final Report to the National Highway Traffic Safety Administration, FH-11-7312, Washington DC, USA

TABC (2007) Statistics of Road Traffic Accidents in PR of China, Traffic Administration Bureau of China, Ministry of Public Security, Beijing, P. R. China

Takahashi Y., Kikuchi Y., Mori F. and Konosu A. (2003) Advanced FE Lower Limb Model for Pedestrians, 18th Int. Technical Conf. on the Enhanced Safety of Vehicles, Nagoya, Japan

Takhounts E.G., Eppinger R.H., Campbell J.Q., Tannous R.E., Power E.D. and Shook L.S. (2003) On the Development of the SIMon Finite Element Head Model, 47th Stapp Car Crash Conf., San Diego, USA

Takhounts E.G., Ridella S.A., Hasija V., Tannous R.E., Campella J.Q., Malone D., Danelson K., Stitzel J., Rowson S. and Duma S. (2008) Investigation of Traumatic Brain Injuries Using the Next Generation of Simulated Injury Monitor (SIMon) Finite Element Model, 52nd Stapp Car Crash Conf., San Antonio, USA

Tosseille X., Tarriere C., Lavaste F., Guillon F. and Domont A. (1992) Development of a FEM of the Human Head according to a Specific Test Protocol, Proc. 30th Stapp Car Crash Conf., pp. 235-253

Turquier F., Kang H.S:, Torsseille X., Willinger R., Lavaste F., Tarriere C. and Domont A. (1996) Validation Study of a 3D Finite Element Head Model Against Experimental Data, 40th Stapp Car Crash Conf., Albuquerque, USA

UNECE (2007) Statistics of Road Traffic Accidents in Europe and North America, United Nations Economic Commission for Europe, http://www.unece.org/trans/main/wp6/pdfdocs/$RAS%202005.pdf, Accessed 2009-09-10

Untaroiu C., Darvish K., Crandall J., Deng B. and Wang J.T. (2005) A Finite Element Model of the Lower Limb for Simulating Pedestrian Impacts, 49th Stapp Car Crash Conf., Washington DC, USA

Vezin, P. and Verriest, J.P. (2005) Development of a Set of Numerical Human Models for Safety, 19th Int. Technical Conf. on the Enhanced Safety of Vehicles, Washington DC, USA

Versace J. (1971) A Review of the Severity Index, 15th Stapp Car Crash Conf., San Diego, USA

Wakim C.F., Capperon S. and Oksman J. (2004) Design of Pedestrian Detection Systems for the Prediction of Car-to-Pedestrian Accidents, 2004 IEEE Intelligent Transportation Systems Conf., Washington DC, USA

Wills K.E., Christoffel K.K., Lavgne J.V., Tanz R.R., Schofer J.L., Donovan M. and Kalangie K. (1997) Patterns and Correlates of Supervision in Child Pedestrian Injury, Journal of Pediatric Psychology, Vol. 22, No., 1, pp. 89-104

Wismans J.S.H.M., Janssen E.G., Beusenberg M., Koppens W.P., Happee R. and Bovendeerd P.H.M. (2000) Injury Biomechanics, Eindhoven University of Technology

Yao J.F., Yang J.K. and Dietmar O. (2008) Investigation of Head Injuries by Reconstruction of Real-World Vehicle-versus-Adult-Pedestrian Accidents, Safety Science, Vol. 46, No. 7, pp. 1103-1114

Yang J.K. (1997) Mathematical Simulation of Knee Responses Associated with Leg Fracture in Car-Pedestrian Accidents, Int. Journal of Crashworthiness, Vol. 2, No. 3, pp. 259-271

Yang J.K. (2003) Pedestrian Head Protection for Car Impacts, Int. Journal of Vehicle Design, Vol. 31, Nos. ½, pp. 16-26

Yang J.K. (2005) Review of Injury Biomechanics in Car-Pedestrian Collisions, Int. Journal of Vehicle Safety, Vol. 1, Nos. 1/2/3, pp. 100-117

Yang J.K., Yao J.F. and Otte D. (2005) Correlation of Different Impact Conditions to the Injury Severity of Pedestrians in Real World Accidents, 19th Int. Technical Conf. on the Enhanced Safety of Vehicles, Washington DC, USA

Yang J.K. and Otte D. (2007) A Comparison Study on Vehicle Traffic Accident and Injuries of Vulnerable Road Users in China and Germany, 20th Int. Technical Conf. on the Enhanced Safety of Vehicles, Lyon, France

Yang J.K., Xu W. and Otte D. (2008) Brain Injury Biomechanics in Real Word Vehicle Accident Using Mathematical Models, Chinese Journal of Mechanical Engineering, Vol. 21, No. 4, pp. 81-86

Zanella A., Butera F., Gobetto E. and Ricerche C. (2002) Smart Bumper for Pedestrian Protection, Smart Materials Bulletin, Vol. 2002, No. 7, pp. 7-9(3)

Zhang L.Y., Yang K.H., Dwarampudi R., Omori K., Li T., Chang K., Hardy W.N., Khali T.B. and King A.I. (2001) Recent Advances in Brain Injury Research: A New Human Head Model Development and Validation, 45th Stapp Car Crash Conf., San Antonio, USA

Zhou C., Khalil T.B. and King A.I. (1995) A New Model Comparing Impact Responses of the Homogeneous and Inhomogeneous Human Brain, 39th Stapp Car Crash Conf, San Diego, USA

Zhou R.G. and Horrey W.J. (2010) Predicting Adolescent Pedestrians' Behavioral Intentions to Follow the Masses in Risky Crossing Situation, Transportation Research Part F, doi: 10.1016/j.trf.2009.12.001